Exact and over-approximated guarantees for corner cutting avoidance in a multi-obstacle environment

Florin Stoican, Ionela Prodan, Esten Ingar Grøtli

Citation:
Florin Stoican, Ionela Prodan, Esten Ingar Grøtli. Exact and over-approximated guarantees for corner cutting avoidance in a multi-obstacle environment. Int. J. Robust. Nonlinear Control, 28, 2018, iss. 15, pp 4528-4548. DOI: https://doi.org/10.1002/rnc.4248

INTERNATIONAL JOURNAL OF ROBUST AND NONLINEAR CONTROL
Int. J. Robust. Nonlinear Control 2010; **00**:1–24
Published online in Wiley InterScience (www.interscience.wiley.com). DOI: 10.1002/rnc

Exact and over-approximated guarantees for corner cutting avoidance in a multi-obstacle environment

Florin Stoican[1], Ionela Prodan[2], Esten Ingar Grøtli[3]

[1] *Department of Automatic Control and Systems Engineering, UPB, Romania (florin.stoican@acse.pub.ro)*
[2]*Laboratory of Conception and Integration of Systems (LCIS EA 3747), Grenoble INP, France (ionela.prodan@lcis.grenoble-inp.fr)*
[3]*Mathematics and Cybernetics, SINTEF Digital, Norway (esteningar.grotli@sintef.no)*

SUMMARY

The corner cutting avoidance problem is an important but often overlooked part of motion planning strategies. Obstacle and collision avoidance constraints are usually imposed at the sampling time without regards to the intra-sample behavior of the agent. Hence, it is possible for an agent to "cut the corner" of an obstacle while apparently respecting the constraints.
This paper improves upon state of the art by providing exact and over-approximated descriptions of the under-shadow (and of its complement, the visible) region generated by an agent against obstacles. We employ a hyperplane arrangement construction to handle multiple obstacles simultaneously, provide piecewise descriptions of the regions of interest and parametrizations of the corner cutting conditions (useful, e.g., in finite horizon optimization problems). Mixed-integer representations are used to describe the regions of interest, leading, in the over-approximated case to binary-only constraints.
Illustrative proofs of concept, comparisons with the state of the art and simulations over a standard multi-obstacle avoidance problem showcase the benefits of the proposed approach. Copyright © 2010 John Wiley & Sons, Ltd.

Received . . .

KEY WORDS: Corner cutting problem, Multi-obstacle avoidance, Hyperplane arrangement, Mixed-Integer Programming (MIP), Model Predictive Control (MPC).

1. INTRODUCTION

Recent advances in computational resources and the proliferation of (semi-)autonomous vehicles has lent new interest to the topic of *obstacle and collision avoidance* in motion planning strategies. One of the major issues is that avoidance constraints lead to a non-convex feasible domain. It is worth underlining that such formulations are intrinsic to the problem and cannot be avoided [1, 2, 3].

This paper concentrates on the "corner cutting" issue: avoidance constraints are checked at each sampling time but the control input is ultimately applied (e.g., via a zero-order hold block) to continuous dynamics. Hence, the intra-sample behavior of the agent (the autonomous vehicle to be steered) cannot be overlooked. While alluring, obstacle enlargement techniques [4] or sampling time reduction are not always appropriate. The former increases the conservatism of the formulation (potentially leading to infeasibility) and the latter reduces the time available for computing the input.

The computational limitations are particularly troublesome since modeling the associated optimization problem is often done via the Mixed-Integer Programming (MIP) framework [5, 6] which scales badly with problem size and complexity (i.e., number of obstacles).

*Correspondence to: Florin Stoican, Department of Automatic Control and Systems Engineering, UPB, Romania. E-mail: florin.stoican@acse.pub.ro

There are many results in the mathematical community related to the *illumination of convex bodies* topic [7] but the emphasis is descriptive rather than constructive. In fact, to the best of our knowledge, there appear to be few results in the control community which describe corner cutting constraints (in either exact or over-approximated form). We are aware of results from [8, 9, 10] which discuss over-approximated corner cutting constraints and provide constructive details: [8] provides the initial construction; [9] and [10] improve it by reducing the number of necessary constraints and by reducing the number of necessary binary variables, respectively.

While interesting, the existing methods, in our opinion, are lacking in several directions:

i) the extension to a multi-obstacle environment is not straightforward;
ii) the underlying structure of the feasible domain is not fully exploited;
iii) constraints involving only binary variables do not describe precisely the position.

The current work is based and expands previous results of the authors. Preliminary results in [11] discuss the corner cutting topic (expanded here with additional theoretical results, comparisons with the state of the art and extensive illustrative examples). [12, 13] discuss the dual problem of coverage in a multi-obstacle environment.

To describe the multi-obstacle environment (issue i)) we propose to use hyperplane arrangements [14]. That is, the domain is partitioned into disjoint cells uniquely characterized by a collection of signs (a "tuple") which are further labeled as *interdicted* – the obstacles or as *admissible* – the feasible space [6].

Next, we provide descriptions for the *shadow region* (and its complement, the *visible region*) spanned by the agent in conjunction with the obstacles. The scaffolding provided by the hyperplane arrangement allows to have piecewise characterizations, i.e., to each admissible cell of the arrangement corresponds a specific shape of the shadow region. Calculating these shapes a priori solves issue ii) and allows to parametrize the corner cutting constraints (necessary for example in a finite horizon optimization problem).

Existing results deal with binary-only constraints (issue iii)). This makes sense in the collision avoidance context since these binary terms are used to constrain the agent's position w.r.t. the obstacle(s). In here, for a better insight, we start with exact representations which are parametrized after the actual position of the agent. For the particular case of bounded polyhedral sets we provide here the exact forms for the under-shadow and visible regions and, from them, deduce the over-approximated forms (which in particular circumstances reduce to the constraints presented in the literature).

Also note that the exact representation (Section 3.1 of this paper) may lead to a qualitatively different behavior. That is, the agent's position can make "jumps" which are interdicted under binary-only formulations (as those given in [8, 9, 10] or Section 3.2). E.g., in the case of a single square-shaped obstacle and binary-only constraints, the agent cannot pass directly between regions separated by more than one of the obstacle's support hyperplanes.

Finally, by exploiting the structure provided by the hyperplane arrangement, we provide mixed-integer descriptions for the regions of interest. That is, using results from [6, 11] together with codification methods found in [15] and the references therein we provide mixed-integer representations which describe both the shadow region and its complement in both the exact and over-approximated forms.

The paper is organized as follows. Section 2 presents the hyperplane arrangement and Section 3 provides the exact and over-approximated representations for the under-shadow and visible regions. Section 4 provides the associated MIP representations and a comparison with the state of the art. An MPC optimization problem is considered in Section 5 and the conclusions are drawn in Section 6.

Notation. The collection of all possible combinations of N binary variables is given by $\{0,1\}^N = \{(b_1,\dots,b_N) : b_i \in \{0,1\}, \forall i = 1\dots N\}$, the same definition holds for sign tuples $\{-,+\}^N$. $\mathrm{Cone}(x,Y) = \{x + \sum_{i:\, y_i \in Y} \beta_i(y_i - x),\ \forall \beta_i \geq 0\}$ denotes the pointed cone spanned from point x and tangent to set Y. $\mathrm{Conv}(X,Y) = \{\alpha x + (1-\alpha)y, \forall x \in X, \forall y \in Y, 0 \leq \alpha \leq 1\}$ is the convex hull of the sets X and Y. $\mathrm{Int}\,(X)$ denotes the interior of set X.

DOI: 10.1002/rnc

2. PRELIMINARIES

Let us consider a finite collection of hyperplanes from $\mathbb{R}^n$, $\mathbb{H} = \{\mathcal{H}_i\}_{i\in\mathcal{I}}$ with

$$\mathcal{H}_i = \left\{x \in \mathbb{R}^n : \; h_i^\top x = k_i\right\}, \; i \in \mathcal{I}, \tag{1}$$

where $\mathcal{I} \triangleq \{1 \dots N\}$ and $(h_i, k_i) \in \mathbb{R}^n \times \mathbb{R}$.

Each of these hyperplanes partitions the space into two disjoint regions (which halve the space and hence are called "half-spaces"):

$$\mathcal{H}_i^+ = \left\{x \in \mathbb{R}^n : \quad h_i^\top x \leq \quad k_i\right\}, \tag{2a}$$
$$\mathcal{H}_i^- = \left\{x \in \mathbb{R}^n : \; -h_i^\top x \leq -k_i\right\}. \tag{2b}$$

Furthermore, hyperplanes (1) cut the space $\mathbb{R}^n$ into disjoint cells

$$\mathcal{A}(\sigma) = \bigcap_{i\in\mathcal{I}} \mathcal{H}_i^{\sigma(i)}, \tag{3}$$

which are feasible intersections of halfspaces (2a)–(2b) with the signs appropriately taken from the sign tuple $\sigma = (\sigma(1), \dots, \sigma(N))$. Such a partitioning of the space is called a hyperplane arrangement and is the union of all cells (3), that is, $\mathbb{R}^n = \mathbb{A}(\mathbb{H}) = \bigcup_{\sigma\in\Sigma} \mathcal{A}(\sigma)$ where $\Sigma \subset \{-,+\}^N$ denotes the collection of all tuples describing non-empty regions (3).

We can then partition the sign tuples into 'admissible' ($\sigma^\circ \in \Sigma^\circ$) and 'interdicted' ($\sigma^\bullet \in \Sigma^\bullet$) where $\Sigma^\circ \cap \Sigma^\bullet = \emptyset$ and $\Sigma^\bullet \cup \Sigma^\circ = \Sigma$. The latter subset describes the obstacles whereas the former describes the complement of the obstacle collection:

$$\mathbb{S} = \bigcup_{\sigma^\bullet\in\Sigma^\bullet} \mathcal{A}(\sigma^\bullet), \quad \mathbb{R}^n \setminus \mathbb{S} = \bigcup_{\sigma^\circ\in\Sigma^\circ} \mathcal{A}(\sigma^\circ). \tag{4}$$

A couple of remarks are in order.

Remark 1. In here, we start with the hyperplane arrangement and label accordingly the cells. Just as well, we may have started with a collection of obstacles, gathered their support hyperplanes and subsequently generated the associated arrangement. An intermediary approach is to consider over-approximations which reduce or keep constant the number of hyperplanes (e.g., via homothetic transformations of some seed shape [16]). ♦

Remark 2. The framework presented here represents an additional layer of complexity to the original problem and may, at a first glance, be considered superfluous. In defense of this we may mention two arguments. First, the framework allows to consider an arbitrary multi-obstacle environment with a unitary notation and description. Second, the hyperplane arrangement serves as an underlying scaffolding to the various constructions presented hereinafter. E.g., the *shadow region* discussed in the next section is piecewise defined over the cells of the arrangement. ♦

For further details about hyperplane arrangements and their use in control problems see the monograph [17].

Illustrative example

For the purpose of illustration let us consider the example depicted in Figure 1. We consider a union of three obstacles in $\mathbb{R}^2$, $\mathbb{S} = S_1 \cup S_2 \cup S_3$ defined by 7 hyperplanes. These partition the space into[†] 29 cells from which 3 describe the obstacles and the rest characterize the feasible space $\mathbb{R}^2 \setminus \mathbb{S}$, as in (4). More precisely, we identify $\Sigma^\bullet = \{\sigma^{\bullet,1}, \sigma^{\bullet,2}, \sigma^{\bullet,3}\}$ such that $S_1 = \mathcal{A}(\sigma^{\bullet,1})$, $S_2 = \mathcal{A}(\sigma^{\bullet,2})$ and $S_3 = \mathcal{A}(\sigma^{\bullet,3})$ for $\sigma^{\bullet,1} = (+-+-+++)$, $\sigma^{\bullet,2} = (--+---+)$ and $\sigma^{\bullet,3} = (++++-+$ $+)$. The remaining 26 feasible tuples are gathered in Σ°.

[†]Note that there may be less feasible tuples than the total number of possible combinations [18].

Prepared using rncauth.cls
DOI: 10.1002/rnc

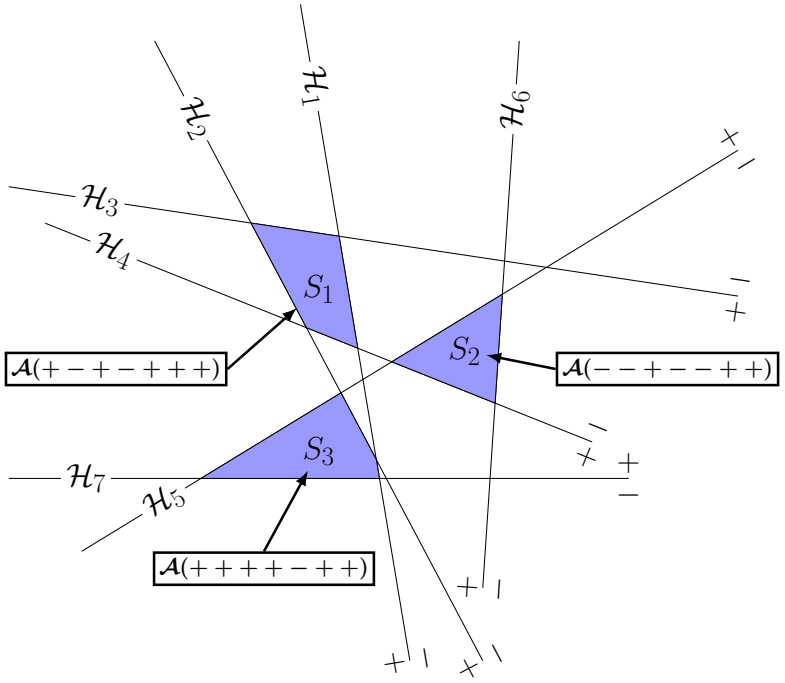

Figure 1. Illustration of a collection of obstacles and their associated hyperplane arrangement.

3. SHADOW REGIONS DESCRIPTIONS

Let us consider a point $x \in \mathbb{R}^n \setminus \mathbb{S}$. Then, the *shadow region* $\mathcal{B}(\mathbb{S}, x)$ given as in [12] is the collection of all the points from $\mathbb{R}^n \setminus \mathbb{S}$ which are not "visible" from x:

$$\mathcal{B}(\mathbb{S}, x) = \{y \in \mathbb{R}^n : [x, y] \cap \mathbb{S} \neq \emptyset\}. \tag{5}$$

This simply states that if the segment $[x, y]$ intersects $\mathbb{S}$ it means that the point y is "hidden" by obstacles $\mathbb{S}$ and therefore is not "visible" from the viewpoint of x.

Remark 3. Definition (5) does not exclude the points $y \in \mathbb{S}$. In other words, the shadow region contains the obstacles as well. We prefer this formulation because it reduces the complexity of the resulting shapes (e.g., if $\mathbb{S}$ is a convex body, then $\mathcal{B}(\mathbb{S}, x)$ is also convex whereas $\mathcal{B}(\mathbb{S}, x) \setminus \mathbb{S}$ may not be). ♦

Considering definition (4), region (5) is rewritten as[‡]

$$\mathcal{B}(\mathbb{S}, x) = \mathcal{B}\left(\bigcup_{\sigma^\bullet \in \Sigma^\bullet} \mathcal{A}(\sigma^\bullet), x\right) = \bigcup_{\sigma^\bullet \in \Sigma^\bullet} \left(\mathcal{B}\left(\mathcal{A}(\sigma^\bullet), x\right)\right) = \bigcup_{\sigma^\bullet \in \Sigma^\bullet} \left(\mathcal{B}\left(\sigma^\bullet, x\right)\right) = \mathcal{B}(\Sigma^\bullet, x). \tag{6}$$

Its complement, the visible region $\overline{\mathcal{B}(\mathbb{S}, x)} = \mathbb{R}^n \setminus \mathcal{B}(\mathbb{S}, x)$ is defined as

$$\overline{\mathcal{B}(\mathbb{S}, x)} = \overline{\mathcal{B}(\Sigma^\bullet, x)} = \overline{\bigcup_{\sigma^\bullet \in \Sigma^\bullet} \mathcal{B}\left(\sigma^\bullet, x\right)} = \bigcap_{\sigma^\bullet \in \Sigma^\bullet} \overline{\mathcal{B}\left(\sigma^\bullet, x\right)}. \tag{7}$$

In what follows we will provide the exact form of $\mathcal{B}\left(\sigma^\bullet, x\right)$, its over-approximation (and of their complements, in the sense of (7)) in a constructive manner which employs the framework from Section 2.

[‡]To shorten the notation, we write $\mathcal{B}\left(\mathcal{A}(\sigma^\bullet), x\right)$ in the compact form $\mathcal{B}\left(\sigma^\bullet, x\right)$. Furthermore, taking into account (4) and the paragraph above it, we use hereafter $\mathcal{B}(\Sigma^\bullet, x)$ as a compact formulation for $\mathcal{B}(\mathbb{S}, x)$.

DOI: 10.1002/rnc

3.1. Exact description of the under-shadow region

The definitions given in (6) and (7) are not amenable to practical implementations. Therefore we need to provide an explicit dependence between the structure of (5) and parameter x. As a first step, we define $\mathbb{V}$, the lattice of points originating from the hyperplane arrangement[§] $\mathbb{H}$:

$$\mathbb{V} = \left\{ v \in \mathbb{R}^n : \; v = \mathcal{H}_{i_1} \cap \cdots \cap \mathcal{H}_{i_{n-1}}, \text{ with } \{i_1, \ldots, i_{n-1}\} \subset \{1, \ldots, N\} \right\}. \tag{8}$$

$\mathbb{V}|_{\mathcal{A}(\sigma^\bullet)}$, the restriction of $\mathbb{V}$ to $\mathcal{A}(\sigma^\bullet)$, denotes the extreme points of $\mathcal{A}(\sigma^\bullet)$. To describe constructively (5), we provide first the following lemma.

Lemma 1. For a forbidden tuple $\sigma^\bullet \in \Sigma^\bullet$ and a point $x \notin \mathcal{A}(\sigma^\bullet)$, the extreme points of $\mathcal{A}(\sigma^\bullet)$ tangent from the point of view of x are given by:

$$\mathcal{E}(\sigma^\bullet, x) = \mathbb{V}|_{\mathcal{A}(\sigma^\bullet)} \cap \left(\bigcup_{i:\, x \notin \mathcal{H}_i^{\sigma^\bullet(i)}} \mathcal{H}_i \right) \cap \left(\bigcup_{j:\, x \in \mathcal{H}_j^{\sigma^\bullet(j)}} \mathcal{H}_j \right). \tag{9}$$

Proof. An extreme point $v \in \mathbb{V}|_{\mathcal{A}(\sigma^\bullet)}$ together with the exterior point x defines a line tangent to the obstacle $\mathcal{A}(\sigma^\bullet)$ if the ray spanned by x and passing through v does not intersect the interior of the obstacle (i.e., $\nexists \beta \geq 0$ s.t. $x + \beta(v - x) \in \mathrm{Int}\,(\mathcal{A}(\sigma^\bullet))$).

Since a ray spanned by x and v either cuts the obstacle or is tangent to it (since $v \in \mathcal{A}(\sigma^\bullet)$), showing that all pairs $(i, j) \notin \{(a, b) : \; x \notin \mathcal{H}_a^{\sigma^\bullet(a)}, \; x \in \mathcal{H}_b^{\sigma^\bullet(b)}\}$ characterize rays which intersect $\mathrm{Int}\,(\mathcal{A}(\sigma^\bullet))$ directly leads to (9). We proceed by assuming that there exists a pair (i, j) s.t. $v \in \mathcal{H}_i \cap \mathcal{H}_j$ and $x \in \mathcal{H}_i^{\sigma^\bullet(i)}$, $x \in \mathcal{H}_j^{\sigma^\bullet(j)}$– the last two inclusions in contradiction with (9). Then, relations $\sigma^\bullet(i) h_i^\top x \leq \sigma^\bullet(i) k_i$, $\sigma^\bullet(i) h_i^\top v \leq \sigma^\bullet(i) k_i$ and $\sigma^\bullet(j) h_j^\top x \leq \sigma^\bullet(j) k_j$, $\sigma^\bullet(j) h_j^\top v \leq \sigma^\bullet(j) k_j$ hold. Taking a scalar β which respects $0 \leq \beta < 1$, we multiply the first (and third) and the second (and fourth) inequalities with $1 - \beta$ and β respectively. This leads to inequalities $\sigma^\bullet(i) h_i^\top [x + \beta(v - x)] \leq \sigma^\bullet(i) k_i$ and $\sigma^\bullet(j) h_j^\top [x + \beta(v - x)] \leq \sigma^\bullet(j) k_j$. Therefore, $x + \beta(v - x) \in \mathcal{H}_i^{\sigma^\bullet(i)} \cap \mathcal{H}_j^{\sigma^\bullet(j)}$. Since $\mathrm{Int}\left(\mathcal{H}_i^{\sigma^\bullet(i)} \cap \mathcal{H}_j^{\sigma^\bullet(j)} \right) \supset \mathrm{Int}\,(\mathcal{A}(\sigma^\bullet))$ there exists a $\beta \in (0, 1)$ arbitrarily close to 1 for which an interior point of $\mathcal{A}(\sigma^\bullet)$ lies on the ray defined by x and v, thus contradicting the initial assumption. The same reasoning can be applied for the case $x \notin \mathcal{H}_i^{\sigma^\bullet(i)}$, $x \notin \mathcal{H}_j^{\sigma^\bullet(j)}$ thus concluding the proof. ■

The next corollary shows that (9) is piecewise constant on the arrangement $\mathbb{A}(\mathbb{H})$.

Corollary 1. For a $\sigma^\circ \in \Sigma^\circ$, the set $\mathcal{E}(\sigma^\bullet, x)$ remains unchanged[¶] for any $x \in \mathcal{A}(\sigma^\circ)$:

$$\mathcal{E}(\sigma^\bullet, \sigma^\circ) = \mathbb{V}|_{\mathcal{A}(\sigma^\bullet)} \cap \left(\bigcup_{i:\, \sigma^\circ(i) \neq \sigma^\bullet(i)} \mathcal{H}_i \right) \cap \left(\bigcup_{j:\, \sigma^\circ(j) = \sigma^\bullet(j)} \mathcal{H}_j \right). \tag{10}$$

Proof. Term (9) is rewritten in form (10) if we note that the indices for which $x \notin \mathcal{H}_i^{\sigma^\bullet(i)}$ and $x \in \mathcal{H}_i^{\sigma^\bullet(i)}$ remain the same for any point taken from $\mathcal{A}(\sigma^\circ)$ and are in fact given by checking whether the regions $\mathcal{A}(\sigma^\bullet)$ and $\mathcal{A}(\sigma^\circ)$ lie on the same (or opposite) sides of the i-th hyperplane. Then, it is straightforward to replace $x \notin \mathcal{H}_i^{\sigma^\bullet(i)}$ with $\sigma^\circ(i) \neq \sigma^\bullet(i)$ and $x \in \mathcal{H}_j^{\sigma^\bullet(j)}$ with $\sigma^\circ(j) = \sigma^\bullet(j)$. ■

With the help of Lemma 1 and Corollary 1 we reach the following proposition.

Proposition 1. For $\sigma^\circ \in \Sigma^\circ$ and an $x \in \mathcal{A}(\sigma^\circ)$, the shadow region $\mathcal{B}(\sigma^\bullet, x)$ is given by:

$$\mathcal{B}(\sigma^\bullet, x) = \left(\mathrm{Cone}\,(x, \mathcal{E}(\sigma^\bullet, \sigma^\circ)) \right) \cap \left(\bigcap_{i:\, \sigma^\circ(i) \neq \sigma^\bullet(i)} H_i^{\sigma^\bullet(i)} \right), \tag{11}$$

[§]Note that we assume the arrangement to be in general position (i.e., no slight perturbation of any of its hyperplanes changes the number of cells, or, in other words: no two hyperplanes coincide or are parallel).

[¶]Hereafter, notation (10) will supersede (9) in order to underline that (9) depends only on σ° and not on any particular $x \in \mathcal{A}(\sigma^\circ)$.

Prepared using rncauth.cls
DOI: 10.1002/rnc

where

$$\mathrm{Cone}\,(x,\mathcal{E}(\sigma^\bullet,\sigma^\circ))=x+\sum_{i:\,v_i\in\mathbb{V}}\beta_i(v_i-x),\ \text{with}\ \begin{cases}\beta_i\geq 0, & v_i\in\mathcal{E}(\sigma^\bullet,\sigma^\circ)\\ \beta_i=0, & v_i\notin\mathcal{E}(\sigma^\bullet,\sigma^\circ)\end{cases}. \tag{12}$$

Proof. Looking at definition (5) we notice that any point $y\in\mathcal{B}(\sigma^\bullet,x)$ has to be part of $\mathrm{Cone}\,(x,\mathcal{A}(\sigma^\bullet))$. Assuming the opposite would mean that the ray $x+\beta(y-x),\beta\geq 0$ never intersects the obstacle $\mathcal{A}(\sigma^\bullet)$, thus contradicting the starting hypothesis that y is "in the shadow" of the obstacle. Additionally, we need to discard from the cone all the points y which sit on the same side of a hyperplane with the initial point x but are on the opposite side wrt the obstacle (the ray spanned from x and passing through y will intersect the obstacle but the segment $[x,y]$ does not intersect it, i.e., the ray has not yet "reached" the obstacle).

These considerations allows us to define $\mathcal{B}(\sigma^\bullet,x)=\mathrm{Cone}\,(x,\mathcal{A}(\sigma^\bullet))\setminus\bigcup_{i:\,x\notin\mathcal{H}_i^{\sigma^\bullet(i)}}\overline{\mathcal{H}_i^{\sigma^\bullet(i)}}$. Using the equivalences $\bigcup_i\overline{A}_i=\bigcap_i A_i$ and $A\setminus B=A\cap\overline{B}$ we have that $\mathcal{B}(\sigma^\bullet,x)=\big(\mathrm{Cone}\,(x,\mathcal{A}(\sigma^\bullet))\big)\cap\left(\bigcap_{i:\,x\notin\mathcal{H}_i^{\sigma^\bullet(i)}}\mathcal{H}_i^{\sigma^\bullet(i)}\right)$. Noting that the cone spanned from x and tangent to $\mathcal{A}(\sigma^\bullet)$ is completely characterized by x and $\mathcal{E}(\sigma^\bullet,x)$ as per Lemma 1 and applying Corollary 1 we reach formulation (11) and thus conclude the proof. ■

A couple of remarks are in order.

Remark 4. In (12) we consider terms which have no influence in the cone formulation (those with $\beta_i=0$) since this will simplify the notation later on, when we will consider multiple obstacles simultaneously. ♦

Remark 5. A half-space representation of (12) is also possible but raises various numerical issues and is not followed here (both representations are nonlinear but the generator form is easier to write in the subsequent MI representations of Section 4). ♦

3.2. *Over-approximation of the shadow region*

Proposition 1 shows that (11) has a piecewise structure and thus, for any x in a given cell $\mathcal{A}(\sigma^\circ)$, at runtime we need only to input the current value of x into (11). While this reduces the computation burden (i.e., the tangent points (10) and the separation hyperplanes are already known and can be introduced directly in (11), thus avoiding a full re-computation of the cone as in (9)), the formulation for the shadow area is still difficult due to $\mathrm{Cone}\,(x,\mathcal{E}(\sigma^\bullet,\sigma^\circ))$. The solution pursued here is to consider an over-approximation of the shadow region.

As a first step, we provide the following lemma.

Lemma 2. For given $\sigma^\bullet\in\Sigma^\bullet$ and $\sigma^\circ\in\Sigma^\circ$ relation

$$\bigcup_{x\in\mathcal{A}(\sigma^\circ)}\mathrm{Cone}\,(x,\mathcal{E}(\sigma^\bullet,\sigma^\circ))\supset\bigcap_{i:\,\sigma^\circ(i)\neq\sigma^\bullet(i)}\mathcal{H}_i^{\sigma^\bullet(i)}, \tag{13}$$

holds.

Proof. Let us assume that for an $x'\in\bigcap_{i:\,\sigma^\circ(i)\neq\sigma^\bullet(i)}\mathcal{H}_i^{\sigma^\bullet(i)}$ and check whether there exists an $x\in\mathcal{A}(\sigma^\circ)$ such that (13) holds. In addition consider an extreme point v of $\mathcal{A}(\sigma^\bullet)$ such that the ray spanned from x' and passing through v is tangent to $\mathcal{A}(\sigma^\bullet)$. We have the inequalities $\sigma^\bullet(i)h_i^\top x'\leq\sigma^\bullet(i)k_i$ and $-\sigma^\bullet(i)h_i^\top v\leq-\sigma^\bullet(i)k_i$. Taking $\beta>1$ and multiplying the first inequality with $(1-\beta)$ and the second with β and adding them leads to $-\sigma^\bullet(i)h_i^\top\left[x'+\beta(v-x')\right]\leq-\sigma^\bullet(i)k_i$. Repeating for all indices $i:\ \sigma^\circ(i)\neq\sigma^\bullet(i)$ means that there exists a point $x=x'+\beta(v-x')$ which lies in $\mathcal{A}(\sigma^\circ)$. Therefore, we conclude that $x'\in\mathrm{Cone}\,(x,\mathcal{E}(\sigma^\bullet,\sigma^\circ))$ and thus we complete the proof. ■

Lemma 2 helps prove the following corollary.

DOI: 10.1002/rnc

Corollary 2. Let there be $\mathcal{B}(\sigma^\bullet, \sigma^\circ) = \bigcup_{x \in \mathcal{A}(\sigma^\circ)} \mathcal{B}(\sigma^\bullet, x)$, the shadow region associated to a feasible tuple $\sigma^\circ \in \Sigma^\circ$. Then, this region depends only on $\sigma^\circ, \sigma^\bullet$ and is described as follows:

$$\mathcal{B}(\sigma^\bullet, \sigma^\circ) = \bigcap_{\sigma^\circ(i) \neq \sigma^\bullet(i)} H_i^{\sigma^\bullet(i)}, \tag{14}$$

Proof. From the definition of $\mathcal{B}(\sigma^\bullet, \sigma^\circ)$, the fact that $\bigcup_i (A_i \cap B) = \left(\bigcup_i A_i\right) \cap B$ and (11) follows that $\mathcal{B}(\sigma^\bullet, \sigma^\circ) = \bigcup_{x \in \mathcal{A}(\sigma^\circ)} \mathrm{Cone}\,(x, \mathcal{E}(\sigma^\bullet, \sigma^\circ)) \cap \bigcap_{\sigma^\circ(i) \neq \sigma^\bullet(i)} H_i^{\sigma^\bullet(i)}$. Using Lemma 2 leads to (14), thus concluding the proof. ■

Remark 6. By using the over-approximation (14) the shadow region not only retains the same structure for any $x \in \mathcal{A}(\sigma^\circ)$ but actually remains constant. Hence, at run-time it is necessary only to identify the currently active tuple σ° and use the corresponding region (14). ♦

From the implementation point of view, we actually need to characterize the "visible" regions[‖] (i.e., the complement of $\mathcal{B}(\sigma^\bullet, x)$ or of $\mathcal{B}(\sigma^\bullet, \sigma^\circ)$) in a multi-obstacle environment.

Corollary 3. For given $\sigma^\bullet \in \Sigma^\bullet$ and $\sigma^\circ \in \Sigma^\circ$, the visible region is given in its

i) exact form:

$$\overline{\mathcal{B}(\sigma^\bullet, x)} = \overline{\mathrm{Cone}\,(x, \mathcal{E}(\sigma^\bullet, \sigma^\circ))} \cup \bigcup_{\sigma^\circ(i) \neq \sigma^\bullet(i)} \mathcal{H}_i^{\sigma^\circ(i)} \tag{15}$$

ii) over-approximated form:

$$\overline{\mathcal{B}(\sigma^\bullet, \sigma^\circ)} = \bigcup_{\sigma^\circ(i) \neq \sigma^\bullet(i)} \mathcal{H}_i^{\sigma^\circ(i)}, \tag{16}$$

Proof: The proof is straightforward and is based on the *de Morgan's laws*: $\overline{A \cap B} = \overline{A} \cup \overline{B}$ and $\overline{A \cup B} = \overline{A} \cap \overline{B}$ and uses definitions (11), (14) and the fact that $\overline{\mathcal{H}_i^{\sigma^\bullet(i)}} = \mathcal{H}_i^{\sigma^\circ(i)}$ whenever $\sigma^\circ(i) \neq \sigma^\bullet(i)$. ■

Remark 7. In general, we may consider the shadow area resulting from a set rather than from a point ($x \in \mathbf{X}$). The only difficulty is to check whether the set $\mathbf{X}$ stays in one or more of the regions (3). Defining $\Sigma_{\mathbf{X}} \triangleq \{\sigma \in \Sigma^\circ : \mathbf{X} \cap \mathcal{A}(\sigma) \neq \emptyset\} \subseteq \Sigma^\circ$ allows to characterize the shadow region (along the lines of Proposition 1 and Corollary 2):

$$\mathcal{B}(\sigma^\bullet, \mathbf{X}) = \bigcup_{x \in \mathbf{X} \cap \mathcal{A}(\sigma_x), \sigma_x \in \Sigma_{\mathbf{X}}} \mathcal{B}(\sigma^\bullet, x), \tag{17a}$$

$$\mathcal{B}(\sigma^\bullet, \Sigma_{\mathbf{X}}) = \bigcup_{\sigma_{\mathbf{X}} \in \Sigma_{\mathbf{X}}} \mathcal{B}(\sigma^\bullet, \sigma_{\mathbf{X}}). \tag{17b}$$

♦

Illustrative example

For the example from Section 2 we illustrate the exact and over-approximated under-shadow regions (just for obstacle $S_1 = \mathcal{A}(\sigma^{\bullet,1})$ in order to keep the figure uncluttered).

As a first step, we consider the point $x_1 \in \mathcal{A}(\sigma)$, with $\sigma = (----+++)$, characterizing the gray-filled cell in Figure 2 (b). Checking the signs for tuples $\sigma^{\bullet,1}$ and σ we note that x_1 shares the same half-spaces with S_1 for indices 2, 4, 5, 6 and 7, while for indices 1 and 3 it sits in the opposite half-spaces. Using this information in (9), or alternatively in (10), we note that the set of tangent points of S_1 from the viewpoint of x_1 is given by $\mathcal{E}(\sigma^{\bullet,1}, x_1) = \mathcal{E}(\sigma^{\bullet,1}, \sigma) = \{\mathcal{H}_2 \cap \mathcal{H}_3, \mathcal{H}_1 \cap \mathcal{H}_4\}$.

[‖] The under-shadow regions are of interest in the dual problem of guaranteed coverage of a multi-obstacle domain [13] - 'how to position a collection of agents such that, overall, no point of the environment remains unobserved'.

DOI: 10.1002/rnc

Having $\mathcal{E}(\sigma^{\bullet,1}, \sigma)$ allows to illustrate in Figure 2 (a), using (11) from Proposition 1, the exact under-shadow region $\mathcal{B}(\sigma^{\bullet,1}, x_1) = \mathrm{Cone}(x_1, \mathcal{E}(\sigma^{\bullet,1}, \sigma)) \cap \left(\mathcal{H}_1^+ \cap \mathcal{H}_3^+\right)$. Note that the half-spaces which separate between the position x_1 and the obstacle S_1 are those with indices 1 and 3, i.e., the indices for which the sign tuples $\sigma^{\bullet,1}$ and σ differ.

To highlight that the structure of the under-shadow region (11) remains constant while the agent's position is taken from the same feasible cell (see Proposition 1) we take $x_2 \in \mathcal{A}(\sigma)$ and note in Figure 2 (a) that, indeed, the tangent points to obstacle S_1 remain those of $\mathcal{E}(\sigma^{\bullet,1}, \sigma)$ and the separating half-spaces are, again, those with indices 1 and 3: $\mathcal{B}(\sigma^{\bullet,1}, x_2) = \mathrm{Cone}(x_2, \mathcal{E}(\sigma^{\bullet,1}, \sigma)) \cap \left(\mathcal{H}_1^+ \cap \mathcal{H}_3^+\right)$.

Lastly, we depict in Figure 2 (b) the over-approximated under-shadow region $\mathcal{B}(\sigma^{\bullet,1}, \sigma) = \mathcal{H}_1^+ \cap \mathcal{H}_3^+ s$ as in (14) from Corollary 2. It can be seen that $\mathcal{B}(\sigma^{\bullet,1}, \sigma)$ contains any region $\mathcal{B}(\sigma^{\bullet,1}, x)$ for $x \in \mathcal{A}(\sigma)$, and in particular for $x \in \{x_1, x_2\}$.

DOI: 10.1002/rnc

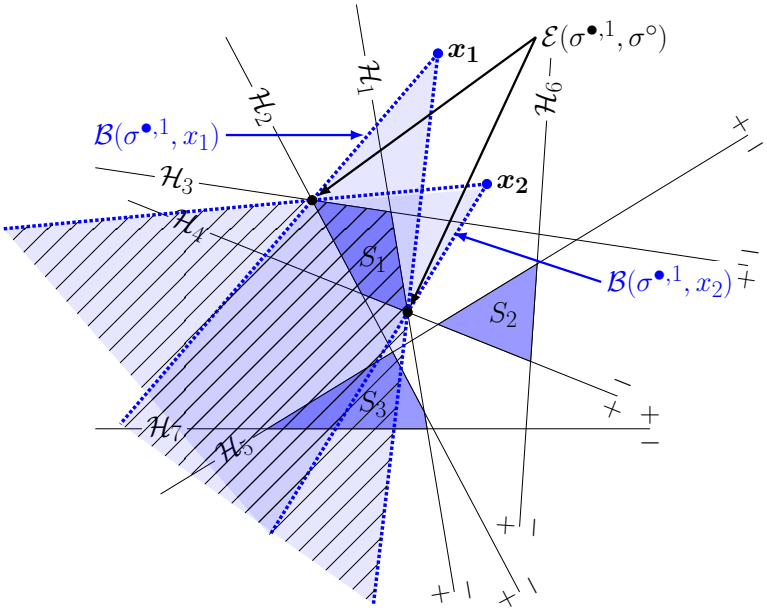

(a) exact case

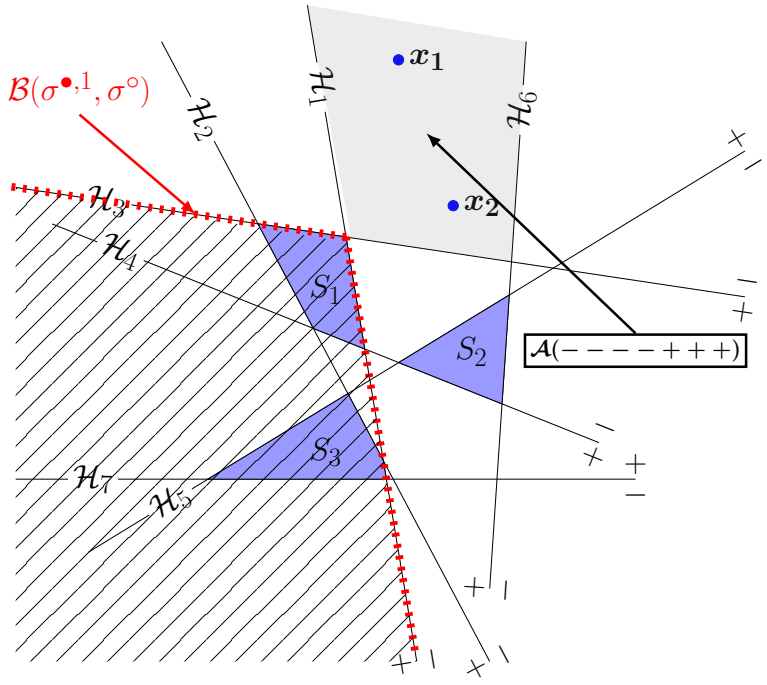

(b) over-approximated case

Figure 2. Illustration of exact and over-approximated under-shadow regions.

DOI: 10.1002/rnc

4. MIXED INTEGER REPRESENTATIONS

In Section 3 we gave various formulations for shadow regions observed from the point of view of an agent and with multiple obstacles. Regardless of the particular construction, the issue is that the resulting feasible region is non-convex (and in the case of multiple obstacles, not even connected). Henceforth, we use mixed integer formulations to express the shadow (and their complements) regions in a manageable form. That is, we add binary variables to the original problem such that the resulting relations describe a pseudo-(non)linear formulation which can be solved with specialized solvers (e.g., CPLEX [19], GUROBI [20] or SCIP [21]).

As a first step, let us consider the Hamming distance $\delta : \{-,+\}^N \times \{-,+\}^N \to \{0,1,\ldots,N\}$ defined between two tuples $\sigma_1, \sigma_2 \in \Sigma$:

$$\delta(\sigma_1,\sigma_2) = \sum_{i:\ \sigma_1(i)\neq\sigma_2(i)} 1. \tag{18}$$

Abusing the notation and equating '-' with '0' and '+' with '1' allows to rewrite (18) as**

$$\delta(\sigma_1,\sigma_2) = |\sigma_1 - \sigma_2| = \sum_i |\sigma_1(i) - \sigma_2(i)| = \sum_i \sigma_1(i) + [1 - 2\sigma_1(i)]\,\sigma_2(i). \tag{19}$$

Remark 8. As long as one of the terms is known (either σ_1 or σ_2), mapping (19) is linear and can be integrated easily in a MI formulation (since the product $\sigma_1(i)\sigma_2(i)$ appearing in (19) has only one variable). ♦

As stated in Remark 8 whenever both tuples σ_1, σ_2 are unknown, mapping (18) is nonlinear, which in turn leads to a mixed integer nonlinear formulation.

This issue can be alleviated through the following lemma (the nonlinear (in)equality is replaced by an enumeration of linear inequalities which is equivalent with the former).

Lemma 3. For $\sigma_1, \sigma_2 \in \Sigma^\circ$ the following equivalencies are true:

$$\Big(|\sigma_1 - \sigma_2| = 0\Big) \leftrightarrow \Big(|\sigma^\circ - \sigma_2| \leq \quad N \cdot |\sigma^\circ - \sigma_1|,\ \forall \sigma^\circ \in \Sigma^\circ\Big), \tag{20a}$$

$$\Big(|\sigma_1 - \sigma_2| > 0\Big) \leftrightarrow \Big(|\sigma^\circ - \sigma_2| > -|\sigma^\circ - \sigma_1|,\ \forall \sigma^\circ \in \Sigma^\circ\Big). \tag{20b}$$

Proof. We consider first the equivalence (20a). The '$\rightarrow$' implication is straightforward, consequently we concentrate on the '$\leftarrow$' implication. The right term of the equivalence (20a) consists of an enumeration of inequalities, one per each feasible sign tuple $\sigma^\circ \in \Sigma^\circ$.

Recalling that $|\sigma^\circ - \sigma_1|$ takes values from $\{0,1,\ldots,N\}$ it follows that the right hand side is zero iff $\sigma^\circ = \sigma_1$ which forces $|\sigma^\circ - \sigma_2| = 0$ and leads to $\sigma_1 = \sigma_2$, the left-part of the equivalence (20a). Whenever $\sigma^\circ \neq \sigma_1$ the right-hand term is large enough to make the inequality redundant (i.e., regardless of the value of $|\sigma^\circ - \sigma_2|$, the inequality holds). A similar reasoning is applied for (20b), thus concluding the proof. ■

Remark 9. Note that (20a)–(20b) are not 'big-M' formulations (see also Remark 10). We are certain that the left-hand sides of the equations cannot be larger than 'N' – the number of hyperplanes and hence we do not need to relax the right-hand term to a value larger than that. ♦

Using constructions similar to the ones in [15] and the references therein we provide in what follows MI formulations for the exact and over-approximated shadow regions (and their complements, the visible regions).

**Since $|\cdot|$ more intuitively denotes the notion of distance, we will henceforth use it instead of notation $\delta(\cdot,\cdot)$.

DOI: 10.1002/rnc

4.1. *Mixed integer representations for the exact shadow and visible regions*

The following proposition gives a MI representation of the exact shadow region from Proposition 1.

Proposition 2. Let there be a point $x \in \mathcal{A}(\sigma)$ and the collection of obstacles characterized by $\Sigma^\bullet$. Then inclusion $x^+ \in \mathcal{B}(\Sigma^\bullet, x) = \bigcup_{\sigma^{\bullet,j} \in \Sigma^\bullet} \mathcal{B}(\sigma^{\bullet,j}, x)$ holds iff

$$x^+ = x + \sum_i \beta(i)(v_i - x),\ \beta(i) \geq 0, \tag{21a}$$

$$\sum_{i:\, v_i \notin \mathcal{E}(\sigma^{\bullet,j}, \sigma^\circ)} \beta(i) \leq M\left(|\sigma^\circ - \sigma| + \alpha^j\right),\ \forall \sigma^\circ \in \Sigma^\circ, \forall \sigma^{\bullet,j} \in \Sigma^\bullet \tag{21b}$$

$$\sigma^{\bullet,j}(\ell) h_\ell^\top x^+ \leq \sigma^{\bullet,j}(\ell) k_\ell + M(1 - \left|\sigma^{\bullet,j}(\ell) - \sigma(\ell)\right| + \alpha^j), \forall \ell = 1 \ldots N, \forall \sigma^{\bullet,j} \in \Sigma^\bullet \tag{21c}$$

$$\sum_j \left(1 - \alpha^j\right) \geq 1, \tag{21d}$$

is feasible. Auxiliary variables $\beta(i) \in \mathbb{R}$, $\alpha^j \in \{0, 1\}$ are taken appropriately.

Proof. Inclusion $x^+ \in \mathcal{B}(\Sigma^\bullet, x)$ means that there should be at least an active obstacle $\mathcal{A}(\sigma^{\bullet,j})$ such that $x^+ \in \mathcal{B}(\sigma^{\bullet,j}, x)$. Proposition 1 shows that this is equivalent with having $x^+ \in \text{Cone}\left(x, \mathcal{E}(\sigma^{\bullet,j}, \sigma^\circ)\right)$ and $x^+ \in \bigcap_{\sigma^\circ(i) \neq \sigma^{\bullet,j}(i)} H_i^{\sigma^{\bullet,j}(i)}$. We proceed to show that these inclusions are equivalent with having (21) feasible.

Auxiliary binary variable α^j marks whether x^+ lies in the shadow region determined by $\sigma^{\bullet,j}$, or not ($\alpha^j = 0$ for the former and $\alpha^j = 1$ for the later). Having $\alpha^j = 1$ means that the right-hand terms from (21b) and (21c) are always greater than the left-hand terms (see also Remark 10). Therefore the inequalities (21b) and (21c) become redundant. (21d) ensures that at least one $\sigma^{\bullet,j}$ is active (i.e., that there exists at least one index 'j' s.t. (21b) and (21c) are not redundant).

Assuming, without loss of generality, that we are in the case $\alpha^j = 0$ we analyze the rest of the terms. (21a) describes the cone spanned from x and passing through extreme points v_i. With the help of Lemma 3, (21b) ensures that only the extreme points which are active for the pair $\left(\sigma, \sigma^{\bullet,j}\right)$ participate in the cone construction (since the terms $\beta(i)$ are positive, if their sum is zero then each term is zero). (21c) adds the half-spaces which separate the obstacle $\mathcal{A}(\sigma^{\bullet,j})$ from the point x. ■

A couple of remarks are in order.

Remark 10. Relations (21) make use of the "big M" representation. That is, we consider (usually in the right hand side of the equation) a combination of binary variables multiplied by a large value (i.e., 'M'). This means that whenever the binary part is ≥ 1 the right hand is for practical purposes infinite thus making the associated inequality redundant. Conversely, when the binary part is zero it means that the inequality remains active and that it constrains the feasible space. ♦

Remark 11. Proposition 2 assumes that the value of x and the value of its sign tuple σ are unknown. This is the reason for which terms '$|\sigma^\circ - \sigma|$' appear in (21b). Similar with the reasoning of Lemma 3, enumerating all feasible tuples $\sigma^\circ \in \Sigma^\circ$ means that, of all the inequalities, just the ones for which $\sigma^\circ = \sigma$ are non-redundant and contribute to the description. Similarly, in (21c), terms '$\left|\sigma^{\bullet,j}(\ell) - \sigma(\ell)\right|$' make sure that only the appropriate half-spaces are taken into consideration.

Conversely, if x, σ are known, the terms mentioned earlier will disappear from formulation (21), leading to a simpler form (with both less inequalities and less variables). ♦

Remark 11 will prove useful later on when we will consider a model predictive control scheme: the associated optimization problem assumes a sequence of predicted values which are not known a priori but are decision variables in the optimization problem.

In Proposition 2 we provided a mixed integer description of the shadow region. Next, we provide its counterpart, the mixed integer description of the visible region.

DOI: 10.1002/rnc

Proposition 3. Let there be a point $x \in \mathcal{A}(\sigma)$ and the collection of obstacles characterized by $\Sigma^\bullet$. Then exclusion $x^+ \notin \mathcal{B}(\Sigma^\bullet, x) = \bigcup_{\sigma^{\bullet,j} \in \Sigma^\bullet} \mathcal{B}(\sigma^{\bullet,j}, x)$ holds iff

$$x^+ = x + \sum_{i:\, v_{j_i} \in \mathbb{V}|_{\mathcal{A}(\sigma^{\bullet,j})}} \beta^j(i)(v_{j_i} - x), \tag{22a}$$

$$|\beta^j(i)| \leq M\left(|\sigma^\circ - \sigma| + 1 - \alpha^j\right),\ i:\ v_i \notin \mathcal{E}(\sigma^{\bullet,j}, \sigma^\circ), \tag{22b}$$

$$\beta^j(i) \leq M\left(1 - \lambda^j(i) + |\sigma^\circ - \sigma| + 1 - \alpha^j\right),\ i:\ v_i \in \mathcal{E}(\sigma^{\bullet,j}, \sigma^\circ), \tag{22c}$$

$$\sum_{i:\, v_{j_i} \in \mathcal{E}(\sigma^{\bullet,j}, \sigma^\circ)} \lambda^j(i) \geq 1,\ \forall \sigma^\circ \in \Sigma^\circ, \forall \sigma^{\bullet,j} \in \Sigma^\bullet, \tag{22d}$$

$$-\sigma^{\bullet,j}(\ell) h_\ell^\top x^+ \leq -\sigma^{\bullet,j}(\ell) k_\ell + M\left(|\sigma^{\bullet,j}(\ell) - \sigma(\ell)| + \rho^j(\ell) + \alpha^j\right),\ \ell = 1 \ldots N, \tag{22e}$$

$$\sum_\ell \rho^j(\ell) \leq N - 1,\ \forall \sigma^{\bullet,j} \in \Sigma^\bullet, \tag{22f}$$

is feasible. Auxiliary variables $\beta^j(i) \in \mathbb{R}$, $\alpha^j, \lambda^j(i), \rho^j(\ell) \in \{0, 1\}$ are taken appropriately[††].

Proof. Exclusion $x^+ \notin \mathcal{B}(\Sigma^\bullet, x)$ is equivalent with $x^+ \in \overline{\mathcal{B}(\Sigma^\bullet, x)} = \bigcap_{\sigma^{\bullet,j} \in \Sigma^\bullet} \overline{\mathcal{B}(\sigma^{\bullet,j}, x)}$. In other words, x^+ has to stay in the visible region[‡‡] described by each of the obstacles. Looking at the j-th obstacle, $\mathcal{A}(\sigma^{\bullet,j})$, and recalling Corollary 3 i) means that $x^+ \in \overline{\text{Cone}\,(x, \mathcal{E}(\sigma^\bullet, \sigma))}$ or $x^+ \in \bigcup_{\sigma(i) \neq \sigma^{\bullet,j}(i)} \mathcal{H}_i^{\sigma(i)}$. We proceed to show that these relations are equivalent with having (22) feasible.

Relations (22a)–(22d) describe the exterior of $\text{Cone}\left(x, \mathcal{E}(\sigma^{\bullet,j}, \sigma^\circ)\right)$: (22a) describes the cone spanning from x and passing through the vertices of the currently active obstacle; the selection of the active coefficients is done in (22b) and (22c)–(22d) force that at least one of these coefficients is negative (thus ensuring that x^+ lies outside of the cone). The term $|\sigma^\circ - \sigma|$ appearing in both (22b)–(22c) means that whenever $\sigma \neq \sigma^\circ$ the coefficients $\beta^j(i)$ are not constrained (see also Remark 11).

Relations (22e)–(22f) describe inclusion $x^+ \in \bigcup_{\sigma(i) \neq \sigma^{\bullet,j}(i)} \mathcal{H}_i^{\sigma(i)}$. Staying inside a union of half-spaces means that at least one of them should not be redundant. This is done through the addition of terms $\rho^j(\ell)$ in (22e) and by constraining them in (22f) such that at least one of them is zero. The terms $|\sigma^{\bullet,j}(\ell) - \sigma(\ell)|$ appearing in (22e) select the half-spaces which contain x but not the obstacle (in order to be in the visible region, x^+ has to lie in at least one of them).

Variables α^j permit to switch between the cone and half-space inclusions. ■

4.2. *Mixed integer representations for the over-approximated shadow regions*

The exact formulations (21a)–(21c) and (22a) –(22f) lead to complex representations. This is due to the presence of term $\text{Cone}(\sigma^\bullet, x)$. If on the other hand we use the over-approximations proposed in Corollary 2 and Corollary 3 ii), we greatly simplify the representations.

Proposition 4. Let there be a point $x \in \mathcal{A}(\sigma)$ and the collection of obstacles characterized by $\Sigma^\bullet$. Then the future position $x^+ \in \mathcal{A}(\sigma^+)$ is constrained as follows:

[††]Notation v_i denotes the indexing of vertices within the current obstacle (i.e., i takes values from 1 to the number of vertices in $\mathbb{V}|_{\mathcal{A}(\sigma^{\bullet,j})}$). This underlines that the auxiliary terms β^j, λ^j have as many elements as there are extreme vertices in the j-th obstacle. Notation v_{j_i} denotes indexing in the collection $\mathbb{V}$.

[‡‡]Note that equations (22) allow non-positive solutions for the terms $\beta^j(i)$, thus letting x^+ lie on the boundary of the shadow region. This can be avoided by the introduction of a small negative constant in the right-hand side of (22c).

DOI: 10.1002/rnc

(i) for $x^+ \in \mathcal{B}(\Sigma^\bullet, \sigma)$:

$$\sum_i |\sigma^{\bullet,j}(i) - \sigma(i)| \cdot |\sigma^{\bullet,j}(i) - \sigma^+(i)| \leq N(1 - \alpha^j),\ \forall \sigma^{\bullet,j} \in \Sigma^\bullet, \tag{23a}$$

$$\sum_j \alpha^j \geq 1, \tag{23b}$$

(ii) for $x^+ \notin \mathcal{B}(\Sigma^\bullet, \sigma)$:

$$\sum_i |\sigma^{\bullet,j}(i) - \sigma(i)| \cdot |\sigma^{\bullet,j}(i) - \sigma^+(i)| > 0,\ \forall \sigma^{\bullet,j} \in \Sigma^\bullet. \tag{24}$$

Proof. For both cases it is a matter of ignoring the constraints related to the term $\mathrm{Cone}(\sigma^\bullet, x)$ which means that we remain with (21c) and (22e)–(22f), respectively. Further, we interpret these constraints in terms of three sign tuples: σ^+ characterizes the shadow/visible region and is constrained by the current position (described by σ) and the obstacles (described by $\sigma^{\bullet,j} \in \Sigma^\bullet$).

For the j-th obstacle, characterized by $\sigma^{\bullet,j}$, let us consider the constraint

$$|\sigma^{\bullet,j}(i) - \sigma(i)| \cdot |\sigma^{\bullet,j}(i) - \sigma^+(i)| = 0. \tag{25}$$

Whenever $\sigma^{\bullet,j}(i)$ and $\sigma(i)$ share the same sign (i.e., $|\sigma^{\bullet,j}(i) - \sigma(i)| = 0$) the value of $\sigma^+(i)$ is not constrained but whenever $\sigma^{\bullet,j}(i)$ and $\sigma(i)$ have opposite signs (i.e., $|\sigma^{\bullet,j}(i) - \sigma(i)| = 1$) we have that $\sigma^+(i)$ is constrained to have the same sign as $\sigma^{\bullet,j}(i)$ (thus making $|\sigma^{\bullet,j}(i) - \sigma^+(i)| = 0$). In other words, we have that $\Big(\sigma^{\bullet,j}(i) \neq \sigma(i)\Big) \rightarrow \Big(\sigma^{\bullet,j}(i) = \sigma^+(i)\Big)$.

For case i), from (14) we have that $x^+ \in \mathcal{B}(\sigma^{\bullet,j}, \sigma)$ is equivalent with checking (25) for each index i. Since the sum of positive terms is zero iff all the terms are zero, we have that $\sum_i |\sigma^{\bullet,j}(i) - \sigma(i)| \cdot |\sigma^{\bullet,j}(i) - \sigma^+(i)| = 0$ is a necessary and sufficient condition for $x^+ \in \mathcal{B}(\sigma^{\bullet,j}, \sigma)$. The addition and constraining of auxiliary binary variables α^j in (23) leads to $x^+ \in \mathcal{B}(\Sigma^\bullet, \sigma)$.

Case ii) is treated similarly: $x^+ \notin \mathcal{B}(\sigma^{\bullet,j}, \sigma)$ means that there should exist at least an index i such that (25) does not hold. Since the sum of positive terms is not zero iff at least a term is not zero, we have that $\sum_i |\sigma^{\bullet,j}(i) - \sigma(i)| \cdot |\sigma^{\bullet,j}(i) - \sigma^+(i)| > 0$ is a necessary and sufficient condition for $x^+ \notin \mathcal{B}(\sigma^{\bullet,j}, \sigma)$. Repeating for all $\sigma^{\bullet,j} \in \Sigma^\bullet$ leads to (24), thus concluding the proof. ■

Recalling Remark 8, we note that (23)–(24) are linear only if σ is known. If σ is itself an unknown parameter we propose the following corollary.

Corollary 4. Let there be a point $x \in \mathcal{A}(\sigma)$ and the collection of obstacles characterized by $\Sigma^\bullet$. Then the future position $x^+ \in \mathcal{A}(\sigma^+)$ is constrained as follows:

(i) for $x^+ \in \mathcal{B}(\Sigma^\bullet, \sigma)$:

$$\begin{gathered}\sum_i |\sigma^{\bullet,j}(i) - \sigma^\circ(i)| \cdot |\sigma^{\bullet,j}(i) - \sigma^+(i)| \leq N\left(|\sigma^\circ - \sigma| + 1 - \alpha^j\right),\ \forall \sigma^{\bullet,j} \in \Sigma^\bullet, \\ \sum_j \alpha^j \geq 1,\end{gathered} \tag{26}$$

(ii) for $x^+ \notin \mathcal{B}(\Sigma^\bullet, \sigma)$:

$$\sum_i |\sigma^{\bullet,j}(i) - \sigma^\circ(i)| \cdot |\sigma^{\bullet,j}(i) - \sigma^+(i)| > -|\sigma^\circ - \sigma|,\ \forall \sigma^{\bullet,j} \in \Sigma^\bullet, \tag{27}$$

for all $\sigma^\circ \in \Sigma^\circ$.

DOI: 10.1002/rnc

Proof. The proof is a direct application of Lemma 3 to the relations of Proposition 4: out of the enumeration of inequalities from (26) and (27) the only ones which are non-redundant are those for which $\sigma^\circ = \sigma$ and these are exactly (23)–(24). ■

Remark 12. In Corollary 4 and earlier we assume $x \in \mathcal{A}(\sigma)$. Such an inclusion implies a link between the variable x and its sign tuple σ. Relations

$$h_i^\top x \leq \quad k_i + M\left[1 - \sigma(i)\right], \tag{28a}$$

$$-h_i^\top x \leq -k_i + M\sigma(i), \tag{28b}$$

force x to sit on one side or the other of the i-th hyperplane, as selected by $\sigma(i)$. Similar relations can be written for $x^+ \in \mathcal{A}(\sigma^+)$. ♦

4.3. Comparison with the state of the art

In what follows we compare with papers [8, 9, 10] which, to a large extent, have motivated the current work. These papers discuss the corner cutting issue and provide constructive details for the constraints which ensure its validation. Note that they only consider what we call here the 'over-approximated case' and therefore the comparison will limit to the results from Section 4.2 only.

The principal ideas of [8], with our notation, are summarized as follows:

i) there exists at least one half-space not containing the obstacle which contains the current and successor positions of the agent:

$$\exists i \text{ s.t. } \sigma(i) = \sigma^+(i) = 0; \tag{29}$$

ii) for each pair of consecutive tuples there exists a collection of constraints such that at least one of them is non-redundant and implies (29):

$$\sum_i \left[1 - \sigma^\circ(i)\right] \sigma^+(i) < N + \sum_i \left[1 - 2\sigma^\circ(i)\right] \sigma(i),\ \forall \sigma^\circ \in \{0,1\}^N. \tag{30}$$

Both (29) and (30) assume a single obstacle ($\Sigma^\bullet = \{\sigma^{\bullet,1}\}$) where, by convention, $\sigma^{\bullet,1}(i) = 1, \forall i$. This implies that $\sum_i \sigma(i) \leq N-1$, $\sum_i \sigma^+(i) \leq N-1$.

For item i), introducing $\sigma^{\bullet,1}$ defined above in (24) of Proposition 4 ii) leads to $\sum_i |1-\sigma(i)| \cdot |1-\sigma^+(i)| > 0$ and, consequently, to the existence of an index i s.t. $|1-\sigma(i)| \cdot |1-\sigma^+(i)| = 1$ which directly implies (29).

For item ii), introducing $\sigma^{\bullet,1}$ in (27) of Corollary 4 ii) leads to $\sum_i |1-\sigma^\circ(i)| \cdot |1-\sigma^+(i)| > -\sum_i |\sigma^\circ(i) - \sigma(i)|, \forall \sigma^\circ \in \Sigma^\circ$. Using (19), the previous inequality becomes $N - \sum_i \sigma^+(i) + \sum_i \sigma^\circ(i)\sigma^+(i) > \sum_i \left[2\sigma^\circ(i) - 1\right] \sigma(i)$. A rearranging of the terms leads immediately to (30). While (30) has many more inequalities than (27), since in both cases the only non-redundant one corresponds to $\sigma = \sigma^\circ$ and $\sigma \in \Sigma^\circ$ it follows that (30) and (27) are equivalent for a single obstacle.

[9] improves on [8] by reducing the number of constraints (30) from 2^N to a more manageable N. This is done by forcing two consecutive positions x, x^+ to respect the same constraint, with our notation: $-h_i^\top x \leq -k_i + M\sigma^+(i)$ and $-h_i^\top x^+ \leq -k_i + M\sigma^+(i)$ for all $i = 1 \ldots N$. This implies that there exists at least one index i s.t. both x and x^+ lie on the same side of the hyperplane (and thus on the opposite side from the obstacle), similar with (29).

In both papers the results are discussed over the single obstacle case and it is not obvious how they are expanded to a multi-obstacle environment (even if examples over such cases appear in the

As before, we equate '$-$' with '0' and '$+$' with '1'. In addition, binary variables σ, σ^+, $1-\sigma^\circ$ stand for $\mathbf{d}[i-1]$, $\mathbf{d}[i]$, $\mathbf{q}$ used throughout [8].

DOI: 10.1002/rnc

papers). We assume that the equations written for the single obstacle case are repeated for each new obstacle. This is both cumbersome and increases the redundancy of the problem (in both the number of constraints and variables).

The issues highlighted above are to a great extent alleviated by the use of the hyperplane arrangement framework proposed in this paper. Foremost, a multi-obstacle environment can be treated coherently with a single set of constraints and the problem itself is significantly more compact: in number of decision variables if some of the hyperplanes are shared between obstacles and in number of constraints by exploiting the fact that not all possible sign combinations lead to non-empty cells. In fact, according to Buck's formula [18], a hyperplane arrangement has at most $\binom{0}{N} + \cdots + \binom{d}{N}$ cells, much less than the 2^N of possible sign combinations.

Lastly, [10] proposes a logarithmic scheme to reduce the number of binary variables involved in the selection of the active hyperplanes, as a direct improvement to [9]. We have not pursued this approach here but we point out to [17] for a comparison of encoding methods in the hyperplane arrangement framework.

Illustrative example

We consider the example from Section 2 and apply it to the results of this section (this time for the multi-obstacle case, with S_1, S_2 and S_3 considered together). Recall that the same and opposite half-space signs between σ and $\sigma^{\bullet,1}$ are $\{2,4,5,6,7\}$ and $\{1,3\}$, respectively. A similar reasoning holds for $\sigma^{\bullet,2}$ ($\{1,2,4,6,7\}$ and $\{3,5\}$) and $\sigma^{\bullet,3}$ ($\{6,7\}$ and $\{1,2,3,4,5\}$). In addition, with the notation from Figure 3, we have that $\mathcal{E}(\sigma^{\bullet,1},\sigma) = \{v_1, v_2\}$, $\mathcal{E}(\sigma^{\bullet,2},\sigma) = \{v_3, v_4\}$ and $\mathcal{E}(\sigma^{\bullet,3},\sigma) = \{v_5, v_6\}$. With these elements we construct both the exact and over-approximated shadow regions (11) and (14), as depicted in Figure 3 and Figure 4, respectively (for $x_1 \in \mathcal{A}(\sigma)$).

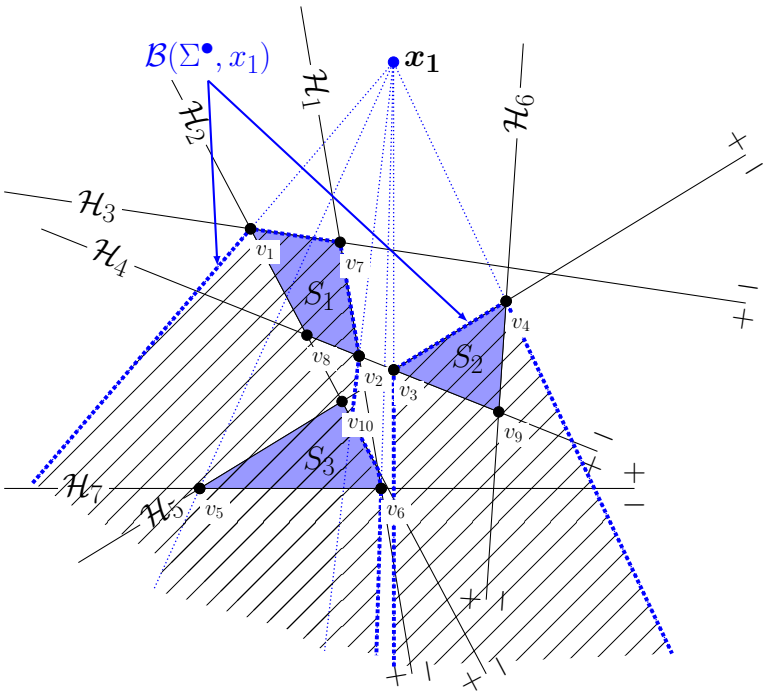

Figure 3. Illustration of the exact shadow region in a multi-obstacle environment.

As illustrated in Figure 3 the exact under-shadow region $\mathcal{B}(\Sigma^\bullet, x_1)$ is rather convoluted: in this particular case, the region is composed from two disjoint pieces, one of them non-convex. Using

DOI: 10.1002/rnc

Proposition 2 we provide the mixed-integer description of this region:

$$x^+ = x + \sum_{i=1}^{10} \beta(i)(v_i - x),\ \beta(i) \geq 0, \quad (31a)$$

$$\beta(3)+\beta(4)+\beta(5)+\beta(6)+\beta(7)+\beta(8)+\beta(9)+\beta(10) \leq M\alpha^1, \quad (31b)$$

$$\beta(1)+\beta(2)+\beta(5)+\beta(6)+\beta(7)+\beta(8)+\beta(9)+\beta(10) \leq M\alpha^2, \quad (31c)$$

$$\beta(1)+\beta(2)+\beta(3)+\beta(4)+\beta(7)+\beta(8)+\beta(9)+\beta(10) \leq M\alpha^3, \quad (31d)$$

$$h_1^\top x^+ \leq k_1 + M\alpha^1, \quad h_3^\top x^+ \leq k_3 + M\alpha^1, \quad (31e)$$

$$h_3^\top x^+ \leq k_3 + M\alpha^2, \quad -h_5^\top x^+ \leq -k_5 + M\alpha^2, \quad (31f)$$

$$h_1^\top x^+ \leq k_1 + M\alpha^3, \quad h_2^\top x^+ \leq k_2 + M\alpha^3,$$
$$h_3^\top x^+ \leq k_3 + M\alpha^3, \quad h_4^\top x^+ \leq k_4 + M\alpha^3,$$
$$-h_5^\top x^+ \leq -k_5 + M\alpha^3, \quad (31g)$$

$$\alpha^1 + \alpha^2 + \alpha^3 \leq 2. \quad (31h)$$

(31a) corresponds to (21a) and constrains the future position of the agent inside the cone determined by the current position. (31b)–(31d) correspond to (21b) and select which of the extreme points are active (e.g, whenever $\alpha^1 = 0$ we have that $\beta(3)+\beta(4)+\beta(5)+\beta(6)+\beta(7)+\beta(8)+\beta(9)+\beta(10) = 0$ which implies that only $\beta(1), \beta(2)$ can be non-zero and thus, (31a) reduces to $x^+ = x + \beta(1)(v_1 - x) + \beta(2)(v_2 - x)$). (31e)–(31g) correspond to (21c) and force the future state x^+ to stay in the half-spaces which separate between the active obstacle and the current position (e.g., whenever $\alpha^1 = 0$, the only active inequalities remain (31e) and these reduce to $h_1^\top x^+ \leq k_1$, $h_3^\top x^+ \leq k_3$ thus forcing the inclusion $x^+ \in \mathcal{H}_1^+ \cap \mathcal{H}_3^+$). Lastly, (31h) corresponds to (21d) and ensures that out of the three obstacles, at least one is active.

Note that for the ease of representation we simplified (21b) in the sense that we wrote only the inequalities corresponding to the case $\sigma^\circ = \sigma$ (otherwise, we should have repeated the group of inequalities (31b)–(31d) for each $\sigma^\circ \in \Sigma^\circ$). Similarly, for (21c) we wrote just these inequalities where the term $|\sigma^{\bullet,j}(\ell) - \sigma(\ell)|$ reduced to zero (such that, e.g., for $j = 1$ we wrote just two inequalities in (31e), instead of seven – the number of hyperplanes).

Proposition 3 provides the mixed-integer description of the visible region $\overline{\mathcal{B}(\Sigma^\bullet, x_1)}$:

$$x^+ = x + \sum_{i=1}^{4} \beta^1(i)(v_{j_i} - x),\ \beta^1(i) \geq 0,\ j_i \in \{1,2,7,8\}, \quad (32a)$$

$$x^+ = x + \sum_{i=1}^{3} \beta^2(i)(v_{j_i} - x),\ \beta^2(i) \geq 0,\ j_i \in \{3,4,9\}, \quad (32b)$$

$$x^+ = x + \sum_{i=1}^{3} \beta^3(i)(v_{j_i} - x),\ \beta^3(i) \geq 0,\ j_i \in \{5,6,10\}, \quad (32c)$$

$$|\beta^1(3)| \leq M\left(1-\alpha^1\right),\ |\beta^1(4)| \leq M\left(1-\alpha^1\right), \quad (32d)$$

$$|\beta^2(3)| \leq M\left(1-\alpha^2\right), \quad (32e)$$

$$|\beta^3(3)| \leq M\left(1-\alpha^3\right), \quad (32f)$$

$$\beta^1(i) \leq M\left(1-\lambda^1(i)+1-\alpha^1\right), \forall i \in \{1,2\}, \quad (32g)$$

$$\beta^2(i) \leq M\left(1-\lambda^2(i)+1-\alpha^2\right), \forall i \in \{1,2\}, \quad (32h)$$

$$\beta^3(i) \leq M\left(1-\lambda^3(i)+1-\alpha^3\right), \forall i \in \{1,2\}, \quad (32i)$$

$$\lambda^1(1)+\lambda^1(2) \geq 1, \quad (32j)$$

$$\lambda^2(1)+\lambda^2(2) \geq 1, \quad (32k)$$

$$\lambda^3(1)+\lambda^3(2) \geq 1, \quad (32l)$$

DOI: 10.1002/rnc

$$-h_1^\top x^+ \le -k_1 + M\left(\rho^1(1) + \alpha^1\right), \quad -h_3^\top x^+ \le -k_3 + M\left(\rho^1(3) + \alpha^1\right), \tag{32m}$$
$$-h_3^\top x^+ \le -k_3 + M\left(\rho^2(3) + \alpha^2\right), \quad h_5^\top x^+ \le k_5 + M\left(\rho^2(5) + \alpha^2\right), \tag{32n}$$
$$-h_1^\top x^+ \le -k_1 + M\left(\rho^3(1) + \alpha^3\right), \quad -h_2^\top x^+ \le -k_2 + M\left(\rho^3(2) + \alpha^3\right),$$
$$-h_3^\top x^+ \le -k_3 + M\left(\rho^3(3) + \alpha^3\right), \quad -h_4^\top x^+ \le -k_4 + M\left(\rho^3(4) + \alpha^3\right),$$
$$h_5^\top x^+ \le k_5 + M\left(\rho^3(5) + \alpha^3\right), \tag{32o}$$
$$1 \ge \rho^1(1) + \rho^1(3), \tag{32p}$$
$$1 \ge \rho^2(3) + \rho^2(5), \tag{32q}$$
$$4 \ge \rho^3(1) + \rho^3(2) + \rho^3(3) + \rho^3(4) + \rho^3(5). \tag{32r}$$

(32a)–(32c) correspond to (22a) and constrain the future position of the agent outside the cones determined by the current position (w.r.t. the obstacles). (32d)–(32f) correspond to (22b) and select which of the extreme points are active in the cone representation (e.g, whenever $\alpha^1 = 0$ we have that $|\beta^1(3)| = 0, |\beta^1(4)| = 0$ which implies that only $\beta^1(1), \beta^1(2)$ can be non-zero and thus, (32a) reduces to $x^+ = x + \beta^1(1)(v_1 - x) + \beta^1(2)(v_2 - x)$). (32g)–(32i) correspond to (22c) and together with (32j)–(32l) which correspond to (22d) ensure that in each of equalities (32a)–(32c) at least one coefficient is negative (such that the future position x^+ is forced to stay outside of the cone).

(32m)–(32o) correspond to (22e) and together with (32p)–(32r) which correspond to (22f) force the future state x^+ to stay in one of the half-spaces which contain the current position but not the active obstacle (e.g., whenever $\alpha^1 = 0$, the inequalities (32m) reduce to $-h_1^\top x^+ \le -k_1 + M\rho^1(1)$, $-h_3^\top x^+ \le -k_3 + M\rho^1(3)$ thus forcing the inclusion $x^+ \in \mathcal{H}_1^- \cup \mathcal{H}_3^-$ since (32p) imposes that at least one of $\rho^1(1), \rho^1(3)$ is zero).

As before, to reduce the number of similar groups of equations which would result from (22), we assumed that we are in the case $\sigma^\circ = \sigma$ and discarded the redundant inequalities (e.g., (32p)–(32r) show only the terms which correspond to non-zero values of the cone coefficients).

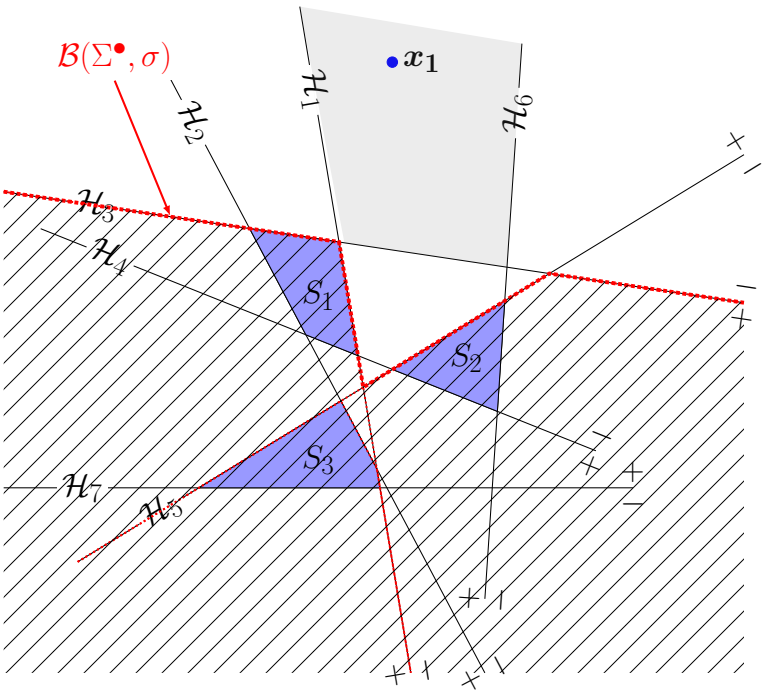

Figure 4. Illustration of the over-approximated shadow regions in a multi-obstacle environment.

DOI: 10.1002/rnc

The over-approximated shadow region $\mathcal{B}(\Sigma^{\bullet}, \sigma)$, defined as in (14), is shown in Figure 4. Using Proposition 4 i) we provide the mixed-integer representation of this region:

$$\left|1-\sigma^{+}(1)\right|+\left|1-\sigma^{+}(3)\right| \leq N(1-\alpha^{1}), \tag{33a}$$

$$\left|1-\sigma^{+}(3)\right|+\left|\sigma^{+}(5)\right| \leq N(1-\alpha^{2}), \tag{33b}$$

$$\left|1-\sigma^{+}(1)\right|+\left|1-\sigma^{+}(2)\right|+\left|1-\sigma^{+}(3)\right|+\left|1-\sigma^{+}(4)\right|+\left|\sigma^{+}(5)\right| \leq N(1-\alpha^{3}), \tag{33c}$$

$$\alpha^{1}+\alpha^{2}+\alpha^{3} \geq 1. \tag{33d}$$

(33a)–(33c) reduce to (23a) by introducing the sign tuples of the obstacles in the formulation. (33d) which corresponds to (23b) forces that at least an obstacle is active. E.g., taking $\alpha^1 = 1, \alpha^2 = \alpha^3 = 0$ means that we remain with (33a) which reduces to $|1-\sigma^{+}(1)|+|1-\sigma^{+}(3)| = 0$. Thus, we have that x^+ can lie in any region which respects $\sigma^{+}(1) = \sigma^{+}(3) = \text{`}+\text{'}$, in other words $x^{+} \in \mathcal{H}_1^{+} \cap \mathcal{H}_3^{+}$.

The over-approximated visible region $\overline{\mathcal{B}(\Sigma^{\bullet}, \sigma)}$, defined as in (16) is written in a mixed-integer representation using Proposition 4 ii):

$$\left|1-\sigma^{+}(1)\right|+\left|1-\sigma^{+}(3)\right| > 0, \tag{34a}$$

$$\left|1-\sigma^{+}(3)\right|+\left|\sigma^{+}(5)\right| > 0, \tag{34b}$$

$$\left|1-\sigma^{+}(1)\right|+\left|1-\sigma^{+}(2)\right|+\left|1-\sigma^{+}(3)\right|+\left|1-\sigma^{+}(4)\right|+\left|\sigma^{+}(5)\right| > 0. \tag{34c}$$

As for (33a)–(33c), we introduce the sign tuples of the obstacles and of the feasible tuple characterizing the current position in (24). In each of the resulting inequalities at least a term has to be strictly positive. E.g., in (34a) we have that $|1-\sigma^{+}(1)| > 0$ and / or $|1-\sigma^{+}(3)| > 0$. Thus, we have that x^+ can lie in any region which does not respect simultaneously $\sigma^{+}(1) = \sigma^{+}(3) = \text{`}+\text{'}$, in other words $x^{+} \in \mathcal{H}_1^{-} \cup \mathcal{H}_3^{-}$. Due to space restrictions and to the fact that the extension to it is simple, we do not exemplify here Corollary 4.

5. STUDY CASE: AN MPC PROBLEM WITH CORNER CUTTING AVOIDANCE

Our corner cutting avoidance procedure is part of an online scheme where collision avoidance is dealt with "as it comes". Alternatives popular in the community consider a priori path planning followed by subsequent tracking (e.g., via command governors [22, 23] or dynamic constraint activation [24]). These approaches have the advantage of guaranteed feasibility (under certain assumptions) but may also make conservative restrictions on the agents allowed positions.

In here, to highlight the corner cutting issue and the guaranteed avoidance constraints discussed earlier we consider a Model Predictive Control (MPC) scheme applied to a double integrator dynamics in the multi-obstacle environment presented in the illustrative examples of the previous sections.

To begin we consider first the continuous-time dynamics (often used in path planning scenarios for reference trajectory generation, [25], [26]):

$$\dot{x}(t) = A_c x(t) + B_c u(t),\ y(t) = C_c x(t), \tag{35}$$

with the state $x(t) \in \mathbb{R}^4$ – composed from position and velocity, input $u(t) \in \mathbb{R}^2$ – the acceleration and the output $y(t) \in \mathbb{R}^2$ – the position component of the state. Matrices A_c, B_c, C_c are given as follows:

$$A_c = \begin{bmatrix} \mathbf{0} & \mathbf{I} \\ \mathbf{0} & \mathbf{0} \end{bmatrix},\ B_c = \begin{bmatrix} \mathbf{0} \\ \mathbf{I} \end{bmatrix},\ C_c = \begin{bmatrix} \mathbf{I} & \mathbf{0} \end{bmatrix}, \tag{36}$$

with $\mathbf{0} \in \mathbb{R}^{2\times 2}$ and $\mathbf{I} \in \mathbb{R}^{2\times 2}$ the 'zero' and 'identity' matrices.

The next step is to consider a sampling time T and give the discrete dynamics associated to (35):

$$x_{k+1} = Ax_k + Bu_k,\ y_k = Cx_k, \tag{37}$$

DOI: 10.1002/rnc

with x_k, u_k and y_k the discrete counterparts of the continuous variables appearing in (35) and matrices A, B, C (obtained via the *zero order hold* method):

$$A = \begin{bmatrix} \mathbf{I} & T \cdot \mathbf{I} \\ \mathbf{0} & \mathbf{I} \end{bmatrix}, \; B = \begin{bmatrix} \frac{T^2}{2} \cdot \mathbf{I} \\ T \cdot \mathbf{I} \end{bmatrix}, \; C = \begin{bmatrix} \mathbf{I} & \mathbf{0} \end{bmatrix}. \tag{38}$$

With these prerequisite we have all the necessary ingredients to formulate the corner cutting avoidance MPC problem:

$$u^* = \underset{u_k, \sigma_{k+1}, \ldots u_{k+N_p-1}, \sigma_{k+N_p}}{\arg\min} \sum_{i=0}^{N_p-1} \|x_{k+i+1}\|_Q + \|u_k\|_R, \tag{39a}$$

$$\text{s.t. } x_{k+i+1} = Ax_{k+i} + Bu_{k+i}. \; y_{k+i} = Cx_{k+i}, \tag{39b}$$

$$x_{k+i} \in \mathcal{X}, \; u_{k+i} \in \mathcal{U}, \tag{39c}$$

$$y_{k+i+1} \notin \mathcal{B}(\Sigma^\bullet, \sigma_{k+i}), \quad i = 0 \ldots N_p - 1, \tag{39d}$$

with N_p, the prediction horizon length; $Q = \text{diag}\,(\mathbf{I}, \mathbf{0})$, $R = \mathbf{I}$, (semi-)positive definite weight matrices for state and input; $\mathcal{X} = \{x : \; |x| \leq \begin{bmatrix} 10 & 10 & 10 & 10 \end{bmatrix}^\top\}$, $\mathcal{U} = \{u : \; |u| \leq \begin{bmatrix} 1 & 1 \end{bmatrix}^\top\}$, bounding sets for state and input.

Standard obstacle avoidance formulations would constrain the output to lie outside the union of obstacles (i.e, $y_{k+i+1} \notin \mathbb{S}$). In (39d) we consider instead the corner cutting avoidance constraint $y_{k+i+1} \notin \mathcal{B}(\Sigma^\bullet, \sigma_{k+i})$ which forces the output to lie outside of the shadow region defined by the obstacles and the current sign tuple.

Note that (39d) describes the over-approximated case: in the sense of (27) from Corollary 4 ii) where y_{k+i}, y_{k+i+1} stand for x, x^+ and constraints $y_{k+i} \in \mathcal{A}(\sigma_{k+i})$, $y_{k+i+1} \in \mathcal{A}(\sigma_{k+i+1})$, implemented as in Remark 12, hold. The exact-case corner cutting avoidance can be implemented by using the exact form of the shadow region: $y_{k+i+1} \notin \mathcal{B}(\Sigma^\bullet, y_{k+i})$, to which correspond the constraints given in Proposition 3.

Note also that the binary variables σ_{k+i} characterizing the predicted output y_{k+i} are unknown and the result of the optimization problem (39). Therefore, for the implementation of the corner cutting avoidance constraints we employ the piecewise descriptions (either as in Proposition 3 – the exact case, or as in Corollary 4 ii) – the over-approximated case).

Lastly, the MPC construction from (39) is relatively simple as it does not implement terminal cost and constraints features. Thus, neither recursive feasibility, nor asymptotic convergence to the origin are guaranteed to hold. We prefer to let the MPC construction in its simplest form and concentrate on the corner cutting aspects, which are the main objective of the paper.

5.1. Justifications for corner cutting avoidance strategies

In what follows we highlight the necessity of corner cutting avoidance strategies by showing that simple obstacle avoidance and even classical methods like obstacle enlargement are unsatisfactorily.

For a sampling time $T = 1$ and horizon length $N_p = 5$ we depict in Figure 5 (a) the trajectories obtained for standard obstacle avoidance and with corner cutting avoidance guarantees (the over-approximated case). While both of them provide feasible values (red circle and 'x' symbols in the figure), when computing the continuous trajectory (via numerical integration of the continuous dynamics to which the discrete input is applied – blue circle and 'x' symbols) we observe that the classic obstacle avoidance trajectory 'cuts' one of the obstacles.

As shown in [9], the continuous $y(t)$ output lies in the region $y_k + \underset{t \in [0,T]}{\text{Conv}}\{tv_k + \frac{t^2}{2}u_k\}$, where v_k denotes the velocity component of the state x_k. In other words, even for a known initial velocity v_k, the next step is uncertain up to the set $\frac{T^2}{2}\mathcal{U}$. Using this set as a safety region (or, equivalently, enlarging the obstacle(s) with the same amount) guarantees corner cutting avoidance. The obstacles thus enlarged are depicted in Figure 5 (b) with dotted contours. As it can be seen, the resulting shapes greatly restrict the feasible domain (in fact, the origin is made infeasible) and increase the

DOI: 10.1002/rnc

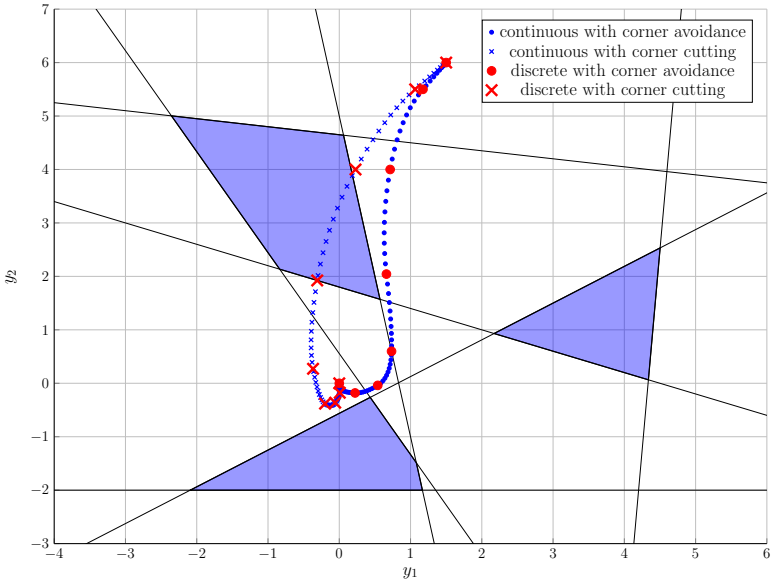

(a) trajectories with and without corner cutting avoidance (with $T = 1$, $N_p = 5$)

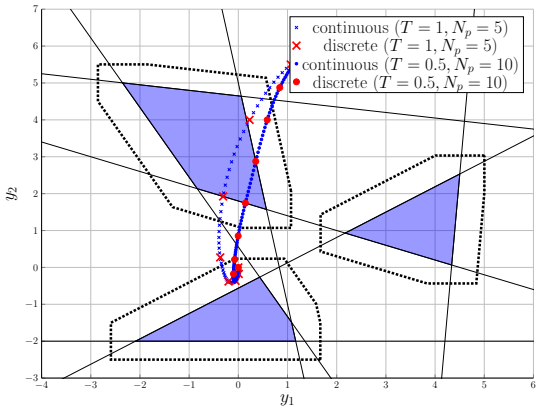

(b) obstacle enlargement (for $T = 1$)

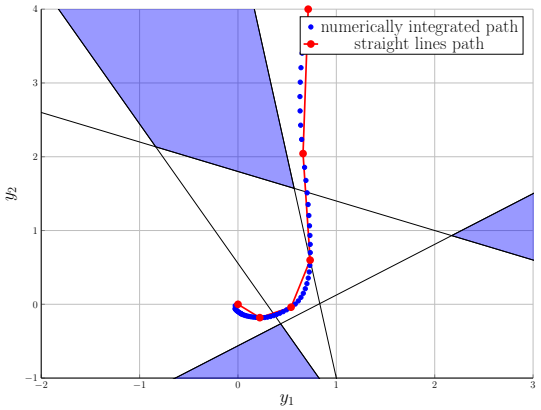

(c) straight line approximation (for $T = 1$)

Figure 5. Inter-sample behavior for double integrator dynamics.

complexity of the problem (the enlargement increases the number of facets which define an obstacle and, consequently, the number of associated binary variables).

Reducing the sampling time may prove useful at first glance (since the safety region decreases proportionally with T^2) but it also means a reduction in available computation time, and, more importantly an increase in the prediction horizon length (decreasing the sampling time means that the horizon length has to increase in order to cover the same continuous time interval). All these caveats means that obstacle enlargement cannot be always employed and that alternatives (such as the strategies proposed in this paper) have to be considered.

Henceforth, we will assume that the agent moves along straight lines in-between consecutive discrete points (see the illustration from Figure 5 (c)). This is a reasonable assumption for a sampling time T small enough. Note that the deviation from a straight line is given by the trajectory's curvature which is much less than its reach. In other words, the size of the safety region which covers the curvature of the trajectory is small enough to be manageable. Note also that in [9] additional constraints are introduced to ensure inter-sample avoidance of the real trajectory of an agent with double integrator dynamics.

DOI: 10.1002/rnc

5.2. *Comparison of various corner cutting avoidance strategies*

In what follows we illustrate in Figure 6 various obstacle avoidance strategies:

S1) standard obstacle avoidance, without corner cutting avoidance guarantees (green triangle);
S2) obstacle avoidance with obstacle enlargement for a safety region $4 \cdot \frac{T^2}{2}\mathcal{U}$ (blue square);
S3) obstacle avoidance with corner cutting avoidance guarantees – the exact case, as in Proposition 3 (black diamond);
S4) obstacle avoidance with corner cutting avoidance guarantees – the over-approximated case, as in Corollary 4 ii) (red circle);

All these strategies are implemented for the aforementioned MPC problem, with initial point $x_0 = \begin{bmatrix} 2 & 2.5 & 2.5 & 0.5 \end{bmatrix}^\top$, sampling time $T = 0.5$, prediction horizon length $N_p = 10$ and use the CPLEX solver [19], except case S3) where the MINLP solver SCIP [21] and a shorter prediction horizon ($N_p = 5$) are used (the latter, due to the excessive size of the problem for the case $N_p = 10$).

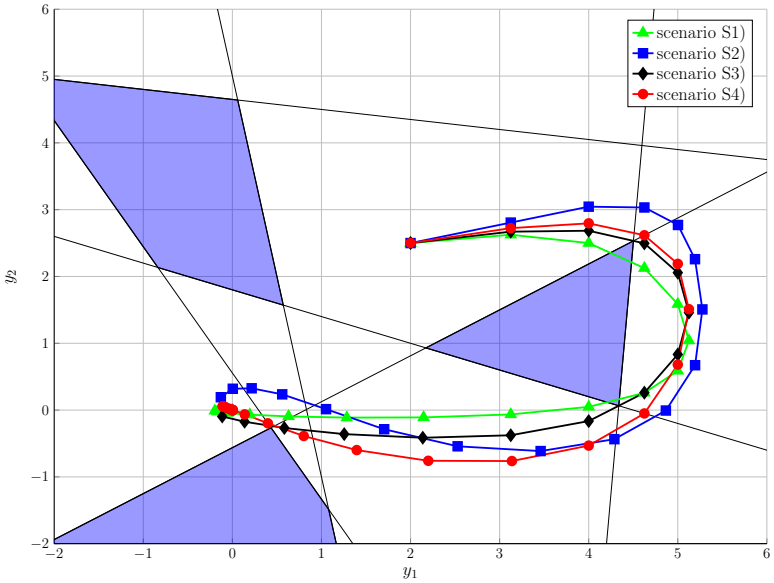

Figure 6. Illustration of trajectories with and without corner cutting avoidance.

Assuming a simulation horizon $N_{sim} = 30$, again with the exception of scenario S3) where a shorter $N_{sim} = 10$ was considered, we obtain that the total simulation times are 0.0957, 0.6353, 11.7452 and 0.0232 respectively. With the caveat that these numbers will change for different values of the problem parameters, we note that scenarios S1) and S4) are comparable, that S2) is an order of magnitude slower than them and that S3) is one order of magnitude slower than S2). Broadly, these results are to be expected: S1) and S4) employ binary-only avoidance constraints and lead to a MILP formulation whereas S2), while still using only binary formulations, does so for a more complex feasible domain (due to the obstacle enlargement procedure). Lastly, S3) with its convoluted nonlinear terms leads to a MINLP formulation and is by far the slowest approach.

To asses the performance of each strategy we measure the total trajectory length* in each case. The results are: 10.0180, 11.5498, 10.1024 and 10.8133, respectively. Again, these values are inline with the expectations: S1) gives the lowest value but does so by cutting the corner of the right-most obstacle; S2) is forced to avoid conservatively the obstacles due to their enlargement; S3) and S4)

*To get the trajectory's length we add the straight-line segments which link the discrete points of the trajectory rather than the 'real' trajectory obtained through numerical integration since the cost appearing in the MPC problem involves only discrete variables.

DOI: 10.1002/rnc

provide the best results (even if, in the case of S3) the prediction horizon is half the size of the one used in S4)).

5.3. *Performance and robustness issues*

To assess the performance and robustness issues of the over-approximated corner cutting avoidance case (strategy S4)) we consider multiple prediction horizon lengths ($N_p \in \{5, 10, 15\}$), sampling times ($T \in \{0.1, 0.5, 1\}$) and the feasible points from within the box $-7.5 \leq y_k \leq 7.5$ spaced with a step of size 1 (there are 245 of them). To each combination of parameters we apply the MPC optimization problem (39) with strategy S4) and observe the various elements of interest (computation time, feasibility of the solution, length of the obtained trajectory).

First, we depict in Table I the mean computation time (averaged over the simulation horizon and over all feasible points) and the maximum time (the largest time spent computing a step in the simulation), respectively. As expected, the computation time (both on average and maximum values)

(a) mean computation time

		T		
		0.1	0.5	1
N_p	5	0.0109	0.0148	0.0169
	10	0.0140	0.0536	0.0685
	15	0.0187	0.1140	0.1630

(b) maximum computation time

		T		
		0.1	0.5	1
N_p	5	0.0200	0.0275	0.0518
	10	0.0434	0.2206	0.2614
	15	0.0517	0.7489	0.9653

Table I. Mean and maximum computation times considered for a 30 steps simulation horizon and for 245 feasible initial conditions.

increases with the length of the prediction horizon[†]. Interestingly, the same can be told about the sampling time. Having a larger sampling time forces a more coarse behavior on the agent: it has to take larger steps and to discard a larger part of the feasible domain (thus leading to more complex computations).

The maximum computation time shows that there are simulation steps for which the difficulty of the problem is markedly increased w.r.t. the average value (e.g., when the agent is near an obstacle and has to judge the optimal path for corner cutting avoidance). To highlight this variation we illustrate in Figure 7 the average and maximum times for each of the 245 initial feasible points in the case $N_p = 10, T = 1$.

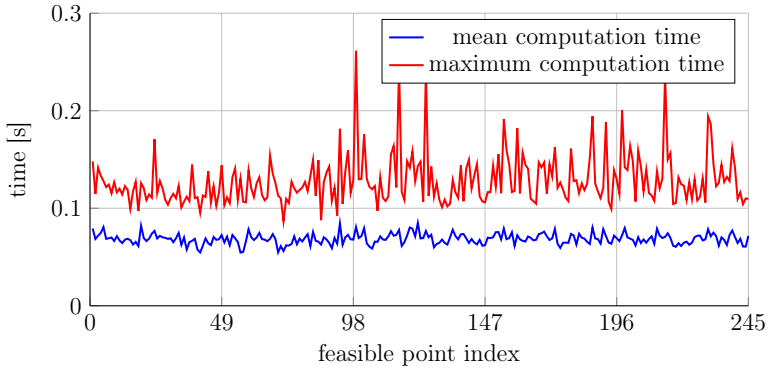

Figure 7. Illustration of mean and maximum computation time for the case ($N_p = 10, T = 1$).

[†]Note that for $N_p = 15, T = 0.5$ there exists at least a sample time at which the computation time exceeds the available time.

DOI: 10.1002/rnc

Another element of interest is the trajectory length from a given starting point. Figure 8 shows the trajectories obtained for each combination of prediction horizon and sampling time: circle, diamond and triangle markers denote the sampling time (0.1, 0.5, 1 respectively) and solid blue, dashed red and loosely dashed green denote prediction horizon (5, 10, 15, respectively) starting from $x = \begin{bmatrix} 5.5 & 2.5 & 0 & 0 \end{bmatrix}^\top$. E.g., a solid blue line with triangle marker denotes the trajectory obtained for parameters $N_p = 5$ and $T = 1$.

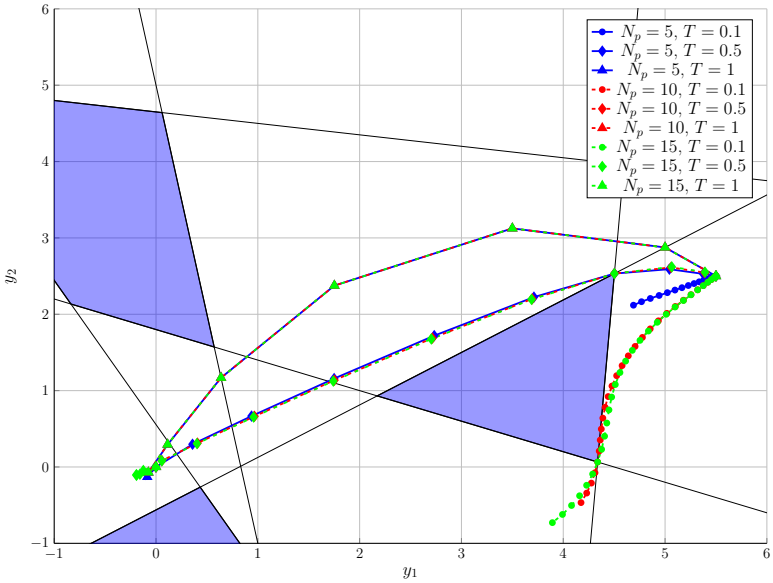

Figure 8. Illustration of path lengths for each feasible initial point.

We observe that the defining element is the sampling time: the trajectories almost coincide for $T = 0.5$ and $T = 1$ and are similar for $T = 0.1$, regardless of the size of the prediction horizon. Furthermore, care should be taken when selecting the sampling time: too small and the trajectory does not reach its destination (the simulation horizon $N_{sim} = 30$ is not enough for the case $T = 0.1$), too large and the trajectory becomes unwieldy (the case $T = 1$).

6. CONCLUSIONS

This paper presented an analysis of the corner cutting avoidance problem for a multi-obstacle environment. Exploiting the underlying structure provided by a hyperplane arrangement, exact and over-approximated forms of the corner cutting avoidance conditions have been provided. We have shown that the mapping of the under-shadow (and of its complement, the visible) region is piecewise defined on the feasible cells of the hyperplane arrangement. Various mixed-integer formulations have been considered and compared with the state of the art. Furthermore, the proposed theoretical results have been implemented in an MPC design in order to show their benefits through simulations and comparison results. Future work will concentrate on using these results in the dual problem: the coverage of a multi-obstacle environment with multiple agents.

ACKNOWLEDGEMENT

The work has been partially funded by a grant of the Romanian National Authority for Scientific Research and Innovation, CNCS UEFISCDI, project number PN-II-RU-TE-2014-4-2713, by a PHC Aurora program, project number 38495XJ and by the Norwegian Research Council through the project with ID 268492/O30.

REFERENCES

1. Richards A, How J. Aircraft trajectory planning with collision avoidance using mixed integer linear programming. *Proceedings of the 21th American Control Conference*, Anchorage, Alaska, USA, 2002; 1936–1941.
2. Schumacher C. UAV task assignment with timing constraints via mixed-integer linear programming. *Technical Report*, Air Force research lab Wright-Patterson AFB of air vehicles directorate 2004.
3. Grundel D, Murphey R, Pardalos P. *Cooperative systems, Control and optimization*, vol. 588. Springer Verlag, 2007.
4. Kuwata Y, How JP. Stable trajectory design for highly constrained environments using receding horizon control. *American Control Conference, 2004. Proceedings of the 2004*, vol. 1, IEEE, 2004; 902–907.
5. Jünger M, Junger M, Liebling T, Naddef D, Nemhauser G, Pulleyblank W. *50 Years of Integer Programming 1958-2008: From the Early Years to the State-of-the-Art*. Springer Verlag, 2009.
6. Prodan I, Stoican F, Olaru S, Niculescu SI. Enhancements on the Hyperplanes Arrangements in Mixed-Integer Techniques. *Journal of Optimization Theory and Applications* 2012; **154**(2):549–572, doi:10.1007/s10957-012-0022-9.
7. Martini H, Soltan V. Combinatorial problems on the illumination of convex bodies. *Aequationes Mathematicae* 1999; **57**(2):121–152.
8. Maia MH, Galvão RKH. On the use of mixed-integer linear programming for predictive control with avoidance constraints. *Int. J. Robust Nonlinear Control* 2009; **19**:822–828, doi:10.1002/rnc.1341.
9. Richards A, Turnbull O. Inter-sample avoidance in trajectory optimizers using mixed-integer linear programming. *Int. J. Robust Nonlinear Control* 2015; **25**:521–526, doi:10.1002/rnc.3101.
10. Afonso RJ, Galvão RK, Kienitz KH. Reduction in the number of binary variables for inter-samp1e avoidance in trajectory optimizers using mixed-integer linear programming. *International Journal of Robust and Nonlinear Control* 2016; **26**(16):3662–3669.
11. Stoican F, Grøtli EI, Prodan I, Oară C. On corner cutting in multi-obstacle avoidance problems. *IFAC-PapersOnLine* 2015; **48**(23):185–190.
12. Strutu MI, Stoican F, Prodan I, Popescu D, Olaru S. A characterization of the relative positioning of mobile agents for full sensorial coverage in an augmented space with obstacles. *Proceedings of the 21st Mediterranean Conference on Control and Automation*, 2013.
13. Stoican F, Prodan I, Strutu MI, Popescu D. Geometrical interpretation on the coverage problems for a mobile agent. *Proceedings of the 18th International Conference on System Theory, Control and Computing, Sinaia, Romania*, 2014; 791–796.
14. Orlik P. Hyperplane arrangements. *Encyclopedia of Optimization*, Floudas CA, Pardalos PM (eds.). Springer US, 2009; 1545–1547.
15. Vielma J, Nemhauser G. Modeling disjunctive constraints with a logarithmic number of binary variables and constraints. *Mathematical Programming* 2011; **128**(1):49–72.
16. Stoican F, Prodan I, Olaru S. Hyperplane arrangements in mixed-integer programming techniques. collision avoidance application with zonotopic sets. *Control Conference (ECC), 2013 European*, IEEE, 2013; 3155–3160.
17. Prodan I, Stoican F, Olaru S, Niculescu SI. *Mixed-integer representations in control design: Mathematical foundations and applications*. Springer, 2015.
18. Buck R. Partition of space. *American Mathematical Monthly* 1943; :541–544.
19. CPLEX II. V12. 1: Users manual for cplex. *International Business Machines Corporation* 2009; **46**(53):157.
20. Optimization G. Inc.,gurobi optimizer reference manual, 2014. *URL: http://www. gurobi. com* 2014; .
21. Maher SJ, Fischer T, Gally T, Gamrath G, Gleixner A, Gottwald RL, Hendel G, Koch T, Lübbecke ME, Miltenberger M, *et al.*. The scip optimization suite 4.0. *Technical Report 17-12*, ZIB, Takustr.7, 14195 Berlin 2017.
22. Franzè G, Lucia W. The obstacle avoidance motion planning problem for autonomous vehicles: A low-demanding receding horizon control scheme. *Systems & Control Letters* 2015; **77**:1–10.
23. Lucia W, Sznaier M, Franze G. An obstacle avoidance and motion planning command governor based scheme: the qball-x4 quadrotor case of study. *Decision and Control (CDC), 2014 IEEE 53rd Annual Conference on*, IEEE, 2014; 6135–6140.
24. Janeček F, Klaučo M, Kalúz M, Kvasnica M. Optiplan: A matlab toolbox for model predictive control with obstacle avoidance. *IFAC-PapersOnLine* 2017; **50**(1):531–536.
25. Grøtli EI, Johansen TA. Path planning for UAVs under communication constraints using SPLAT! and MILP. *Journal of Intelligent and Robotic Systems* 2012; **65**(1-4):265–282, doi:10.1007/s10846-011-9619-8.
26. Grancharova A, Grøtli EI, Ho DT, Johansen TA. UAVs trajectory planning by distributed MPC under radio communication path loss constraints. *Journal of Intelligent and Robotic Systems* 2014; doi:10.1007/s10846-014-0090-1.